AD-A157 024   LIFT DISTRIBUTION ON A HIGH ASPECT RATIO CIRCULATION   1/1
               CONTROL WING WITH RO..(U) DAVID W TAYLOR NAVAL SHIP
               RESEARCH AND DEVELOPMENT CENTER BET.. R J FUREY JUN 85
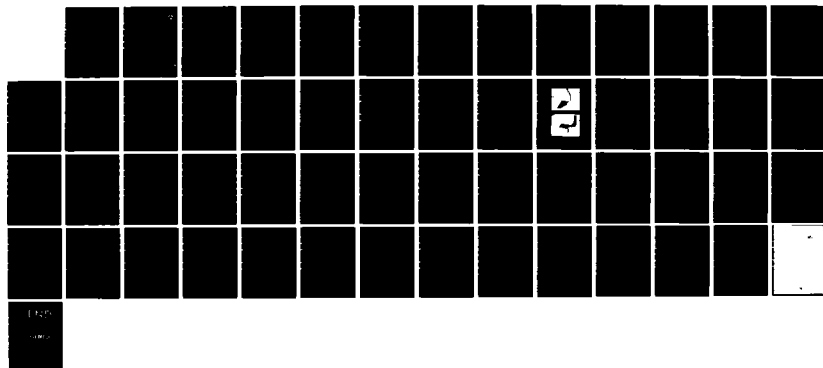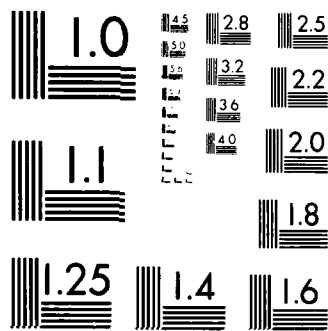UNCLASSIFIED   AERO-1294 DTNSRDC-85/030   F/G 20/4   NL

MICROCOPY RESOLUTION TEST CHART

1.0

1.1

1.25   1.4   1.6

2.8   2.5

3.2

3.6

4.0   2.0

1.8

2.2

AD-A157 024

DAVID W. TAYLOR NAVAL SHIP
RESEARCH AND DEVELOPMENT CENTER

Bethesda, Maryland 20084-5000

LIFT DISTRIBUTION ON A HIGH ASPECT RATIO CIRCULATION
CONTROL WING WITH ROOT LIFT CUTOUT

by

Roger J. Furey

APPROVED FOR PUBLIC RELEASE: DISTRIBUTION UNLIMITED

AVIATION AND SURFACE EFFECTS DEPARTMENT
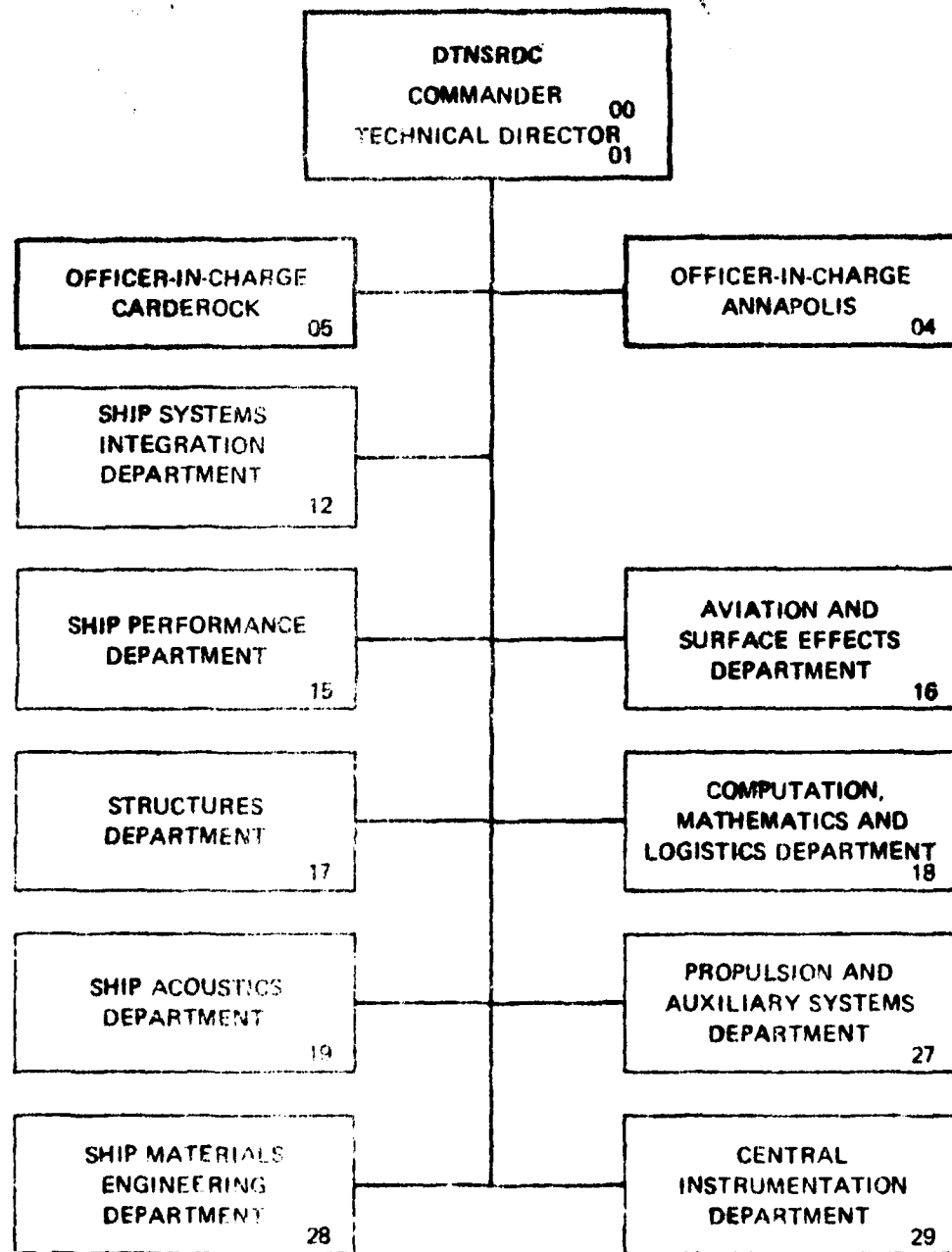RESEARCH AND DEVELOPMENT REPORT

SELECTED
AUG 1 1985

A

1985

DTNSRDC-85/030

85 7 18 001

MAJOR DTNSRDC ORGANIZATIONAL COMPONENTS

```
                    +--------------------------+
                    |        DTNSRDC           |
                    |   COMMANDER          00  |
                    |   TECHNICAL DIRECTOR     |
                    |                      01  |
                    +--------------------------+
```

OFFICER-IN-CHARGE CARDEROCK 05	OFFICER-IN-CHARGE ANNAPOLIS 04
SHIP SYSTEMS INTEGRATION DEPARTMENT 12	
SHIP PERFORMANCE DEPARTMENT 15	AVIATION AND SURFACE EFFECTS DEPARTMENT 16
STRUCTURES DEPARTMENT 17	COMPUTATION, MATHEMATICS AND LOGISTICS DEPARTMENT 18
SHIP ACOUSTICS DEPARTMENT 19	PROPULSION AND AUXILIARY SYSTEMS DEPARTMENT 27
SHIP MATERIALS ENGINEERING DEPARTMENT 28	CENTRAL INSTRUMENTATION DEPARTMENT 29

REPORT DOCUMENTATION PAGE

1a REPORT SECURITY CLASSIFICATION	1b. RESTRICTIVE MARKINGS
UNCLASSIFIED	

2a SECURITY CLASSIFICATION AUTHORITY	3 DISTRIBUTION / AVAILABILITY OF REPORT
2b DECLASSIFICATION / DOWNGRADING SCHEDULE	APPROVED FOR PUBLIC RELEASE: DISTRIBUTION UNLIMITED

4 PERFORMING ORGANIZATION REPORT NUMBER(S)	5 MONITORING ORGANIZATION REPORT NUMBER(S)
DTNSRDC-85/030	Aero Report 1294

6a NAME OF PERFORMING ORGANIZATION	6b OFFICE SYMBOL (If applicable)	7a. NAME OF MONITORING ORGANIZATION
David W. Taylor Naval Ship R&D Center	1660	

6c ADDRESS (City, State, and ZIP Code)	7b ADDRESS (City, State, and ZIP Code)
Bethesda, Maryland 20084-5000	

8a NAME OF FUNDING / SPONSORING ORGANIZATION	8b OFFICE SYMBOL (If applicable)	9 PROCUREMENT INSTRUMENT IDENTIFICATION NUMBER
DTNSRDC	012	

8c ADDRESS (City, State, and ZIP Code)	10 SOURCE OF FUNDING NUMBERS			
	PROGRAM ELEMENT NO	PROJECT NO	TASK NO.	WORK UNIT ACCESSION NO
Bethesda, Maryland 20084-5000	61152N	ZR02302	ZR0230201	

11 TITLE (Include Security Classification)

LIFT DISTRIBUTION ON A HIGH ASPECT RATIO CIRCULATION CONTROL WING WITH ROOT LIFT CUTOUT

12 PERSONAL AUTHOR(S)

Roger Joseph Furey

13a TYPE OF REPORT	13b TIME COVERED		14 DATE OF REPORT (Year, Month, Day)	15 PAGE COUNT
Final	FROM 821001	TO 831001	1985 June	52

16 SUPPLEMENTARY NOTATION

17 COSATI CODES			18 SUBJECT TERMS (Continue on reverse if necessary and identify by block number)
FIELD	GROUP	SUB-GROUP	Circulation Control Wing Lifting Line
			Coanda Surface High Aspect Ratio

19 ABSTRACT (Continue on reverse if necessary and identify by block number)

A computational procedure is developed, based on lifting line theory, which successfully predicts the spanwise lift distribution at moderate blowing momentum coefficient on a high aspect ratio (AR ≈ 18) circulation control wing-body model with several variations in the spanwise extent of blowing. Experimental data are presented on the spanwise lift distribution which validates this procedure.

AUG 1 1985

20 DISTRIBUTION / AVAILABILITY OF ABSTRACT	21 ABSTRACT SECURITY CLASSIFICATION
☐ UNCLASSIFIED/UNLIMITED ☒ SAME AS RPT ☐ DTIC USERS	UNCLASSIFIED

22a NAME OF RESPONSIBLE INDIVIDUAL	22b TELEPHONE (Include Area Code)	22c OFFICE SYMBOL
Roger Joseph Furey	(202) 227-1476	1660

DD FORM 1473, 84 MAR   83 APR edition may be used until exhausted   SECURITY CLASSIFICATION OF THIS PAGE

All other editions are obsolete   UNCLASSIFIED

TABLE OF CONTENTS

LIST OF FIGURES

iv

NOTATION

A_n	Coefficients for fundamental equation, Equation (5)
a_0	Lift curve slope; C_L/α
b	Wing span
b'	Span for blown wing segment
C_L	Aerodynamic lift coefficient
C_{L_T}	Total lift coefficient
C_p	Pressure coefficient; $C_p = (P-P_\infty)/qS$
C_μ	Blowing momentum coefficient; $C_\mu = \dot{m}\,V_j/qS$
c	Wing chord
c_0	Wing root chord
$\bar{c}$	Wing mean chord
d	Fuselage diameter
$f(x)$	Fuselage parameter
h	Coanda jet slot height
J	Thrust
L	Aerodynamic lift force
L_T	Total lift force
$\dot{m}$	Mass flow
P	Pressure
q	Dynamic pressure
r	Radius
r_{te}	Trailing edge radius

S	Wing reference area
s	Wing semispan
s_b	Wing semispan with blowing
t	Wing thickness
V	Velocity
V_J	Jet velocity
V_{LE}	Velocity at the leading edge perpendicular to the chord line
V_∞	Free stream velocity
w_i	Downwash velocity
x	Chordwise coordinate
y	Spanwise coordinate
y_{cc}	Blowing span coordinate
α	Angle of attack
α_c	Camber induced incidence
α_{cc}	Blowing or circulation induced incidence
α'_{cc}	Two-dimensional blowing induced incidence
α_e	Effective incidence
α_g	Geometric incidence
α_i	Induced incidence
α_{icc}	Blowing induced downwash
Γ	Circulation
ΔC_p	Pressure coefficient difference; $(C_{p_\ell} - C_{p_u})$

δ Jet thickness

θ Cylindrical coordinate

λ Wing taper ratio

σ Defined in Equation (8)

ρ Density

ABSTRACT

A computational procedure is developed, based on
lifting line theory, which successfully predicts the
spanwise lift distribution at moderate blowing momentum
coefficient on a high aspect ratio (AR = 18) circulation
control wing-body model with several variations in the
spanwise extent of blowing. Experimental data are
presented on the spanwise lift distribution which validates
this procedure.

ADMINISTRATIVE INFORMATION

INTRODUCTION

The lifting line theory has proven to be quite effective in modeling the spanwise
lift distribution of moderate-to-high aspect ratio wings. The linear nature of the
theory makes it possible to additively incorporate such features as a continuously
varying wing twist, a partial span trailing edge flap, or a jet flap. The current
effort is an attempt to expand on the jet flap model by modifying it to incorporate
the additional feature of lift augmentation produced by a trailing edge Coanda jet.
As with the jet flap, the increased circulation, or effective incidence, produced by
the Coanda jet can be additively included in a lifting line model. The model will
also include the effects of the body on the lift distribution of a circulation
control wing-body configuration.

The Prandtl lifting line theory, as formulated in Thwaites,[1*] will provide the
basis for this model. The three-dimensional jet flap model of Maskell and Spence[2]
will be incorporated and modified to account for a full or partial span trailing edge
Coanda jet. The effect of the fuselage on the flow field will be accounted for in a
manner similar to that of Flax[3] where the potential in the Treftz plane provides for
the wing-body interference. The two-dimensional analysis, provided at a series of
spanwise stations, will account for the effects of blowing rate, trailing edge
radius, thickness effects, camber, and wing taper.

---

*A complete listing of references is given on page 43.

... and easily modified, X-wing model provided the experimental data to ... spanwise lift distribution on a high aspect ratio circulation control ... This report presents selected experimental results and a ... the approximate numerical model.

WING-BODY NUMERICAL MODEL

... field of a wing with trailing edge blowing can be represented, ... and Spence,[2] as experiencing a total lift that consists of ... lift plus a component of thrust from the trailing edge blowing.

$$L_T - J \alpha_{i_o} = \pi \rho V^2 \alpha_{i_\infty} b^2$$

... application of this concept provides for compatibility with Spence's[4] ... of the two-dimensional jet flap.

The above reduces to the familiar

$$L = \rho V \Gamma b$$

In coefficient form the local aerodynamic lift is then:

$$C_L = a_o (\alpha_g + \alpha_c + \alpha_{cc} - \alpha_i) = \left(\frac{2\Gamma}{Vc} \right) \qquad (1)$$

... the angles contributing to the local incidence represent the ... camber, circulation, or blowing induced incidence and downwash. In keeping with the small angle assumptions of the lifting line theory, it is assumed that the sum of the geometric, camber, and circulation induced incidences remains small. The base of blowing ordinarily used on a circulation control wing is low ... that of a jet flap. This condition makes the small angle assumption reasonable and does not create a conflict with the follow-on and usual ... downwash at the wing to that far downstream.

$$\alpha_i = 2 \alpha_{i_o} \qquad (2)$$

The usual procedures for determining the downwash at the wing are then applicable. Equation (1) can be written as:

$$\Gamma = 1/2 \ a_o C \ \{V_\infty(\alpha_g + \alpha_c + \alpha_{cc}) - w_i(y)\} \tag{3}$$

The effect of the fuselage on spanwise lift distribution will be treated according to Flax.[3] Flax transforms the two-dimensional vorticity distribution of the wing-body into the wake contour in the Treftz plane. The result shows itself as a modification to Prandtl's downwash equation in the form:

$$w_i(y) = \frac{1 + f(y)}{4\pi} \int_{-b/2}^{b/2} \frac{d\Gamma}{dy} \frac{dy}{(y'-y)} \tag{4}$$

where $f(y)$ accounts for the fuselage interference and, in the case of a circular fuselage, takes the form $f(y) = (2y/d)^{-2}$.

Introducing a change of variables through the relation:

$$y = \left(\frac{b}{2}\right) \cos \theta$$

a Treftz plane solution, as developed in Karamcheti[5] for example, provides:

$$\Gamma(\theta) = 2b \ V_\infty \sum_{n=1}^{\infty} A_n \sin \theta \tag{5}$$

which, when substituted into Equation (4), gives:

$$w_i(\theta) = V_\infty \ [1+f(y)] \sum_{n=1}^{\infty} n \ A_n \frac{\sin n\theta}{\sin \theta} \tag{6}$$

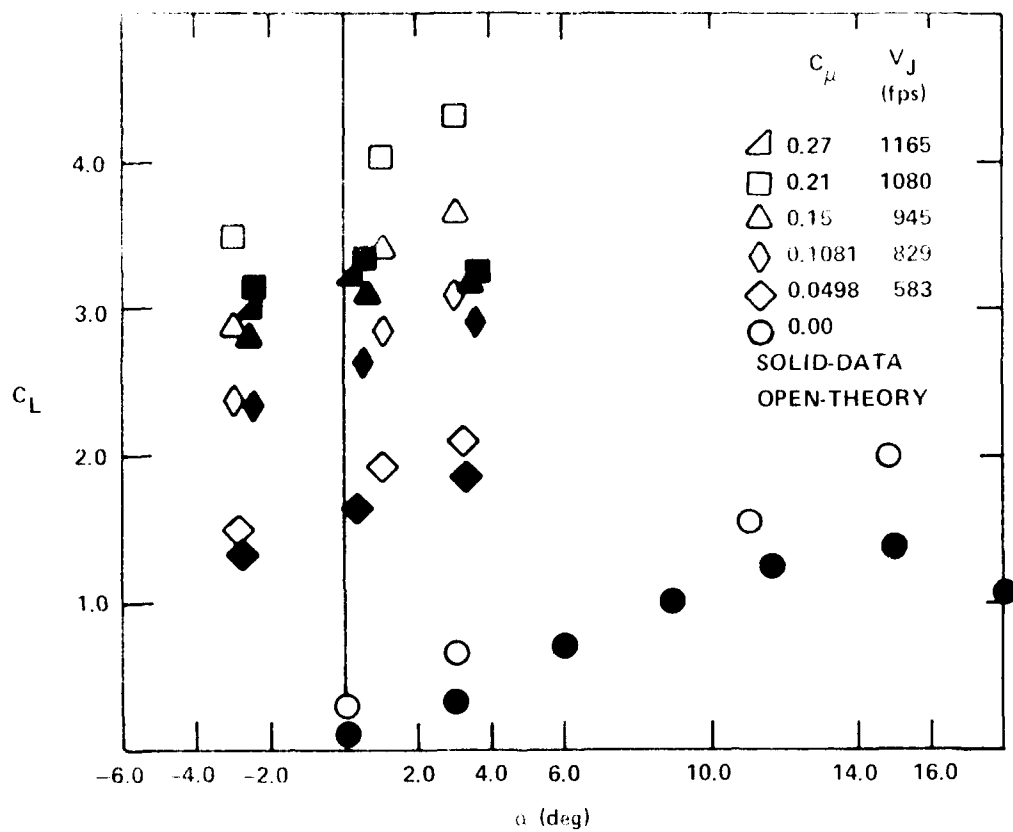Substituting Equations (5) and (6) into (3) provides the fundamental equation:

3

C_μ   V_J (fps)

◁ 0.27   1165
▢ 0.21   1080
△ 0.15   945
◇ 0.1081   829
◇ 0.0498   583
○ 0.00

SOLID-DATA

OPEN-THEORY

C_L

4.0

3.0

2.0

1.0

-6.0   -4.0   -2.0   2.0   4.0   6.0   10.0   14.0   16.0

α (deg)

Figure 21 - Theoretical and Experimental Lift Coefficient, Configuration 1
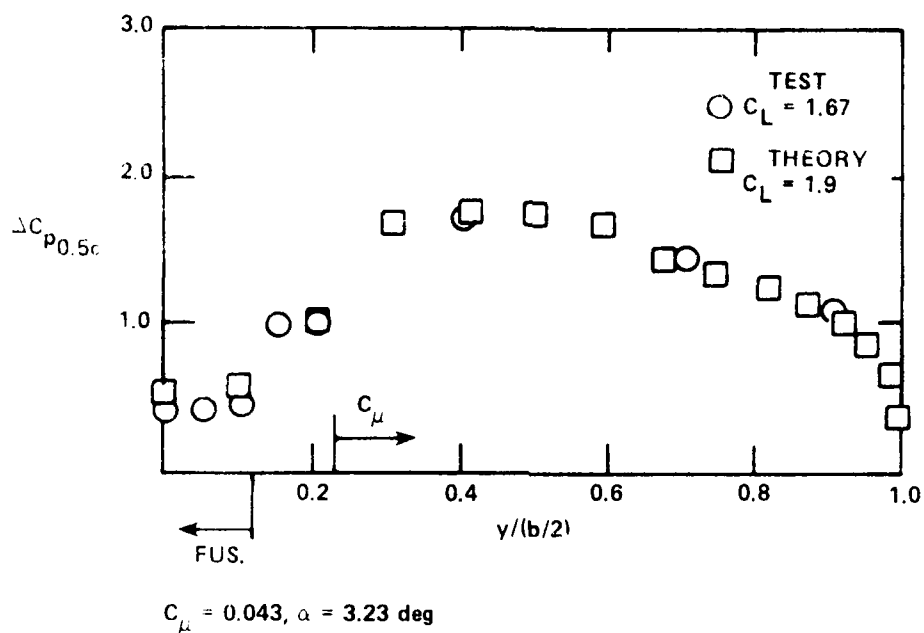
17

$C_\mu = 0.043$, $\alpha = 3.23$ deg

Figure 9 – Spanwise Lift Distribution, Configuration 3, 0.7744 Span Blowing
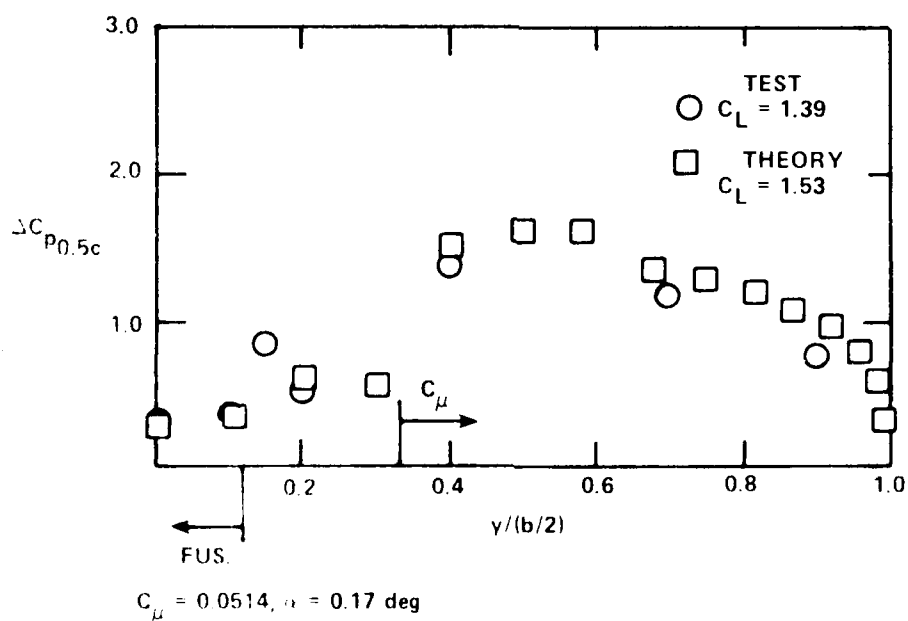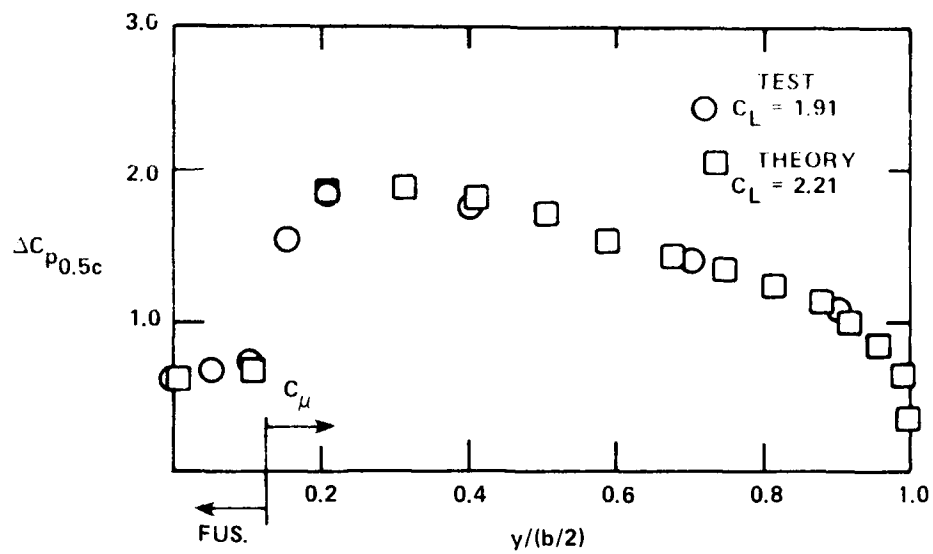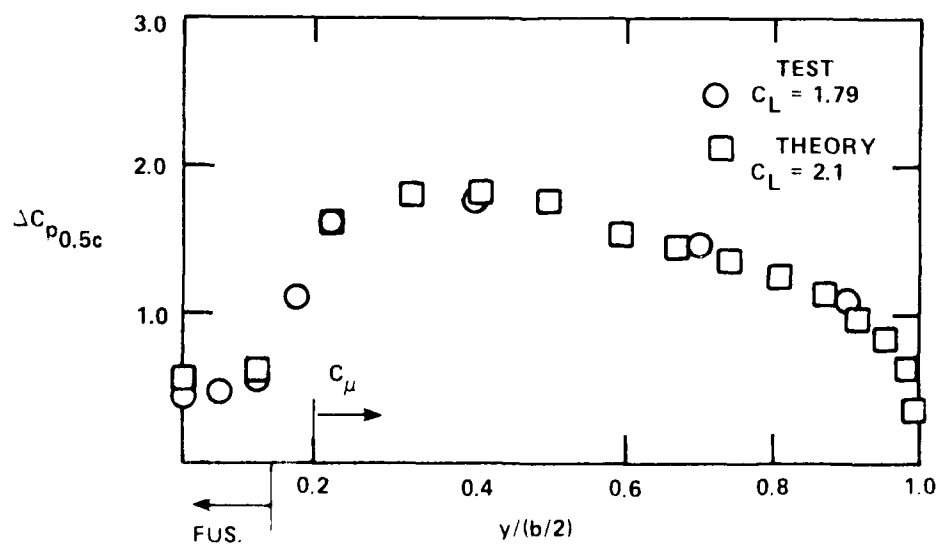

$C_\mu = 0.0514$, $\alpha = 0.17$ deg

Figure 10 – Spanwise Lift Distribution, Configuration 4, 0.675 Span Blowing

$C_\mu = 0.049$, $\alpha = 3.27$ deg

Figure 7 - Spanwise Lift Distribution, Configuration 1, Full Span Blowing

$C_\mu = 0.047$, $\alpha = 3.26$ deg

Figure 8 - Spanwise Lift Distribution, Configuration 2, 0.8249 of Span Blowing
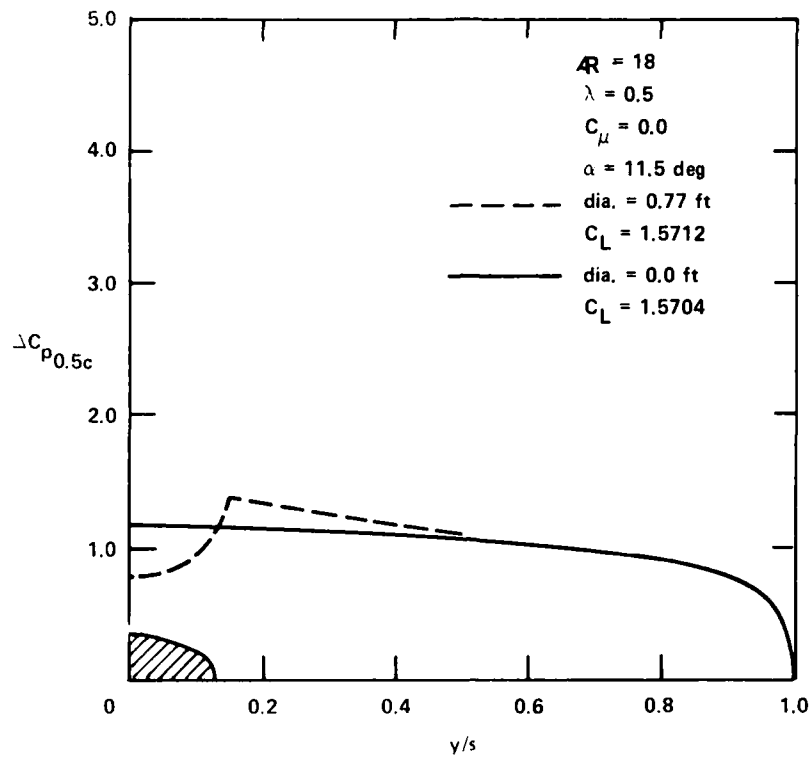
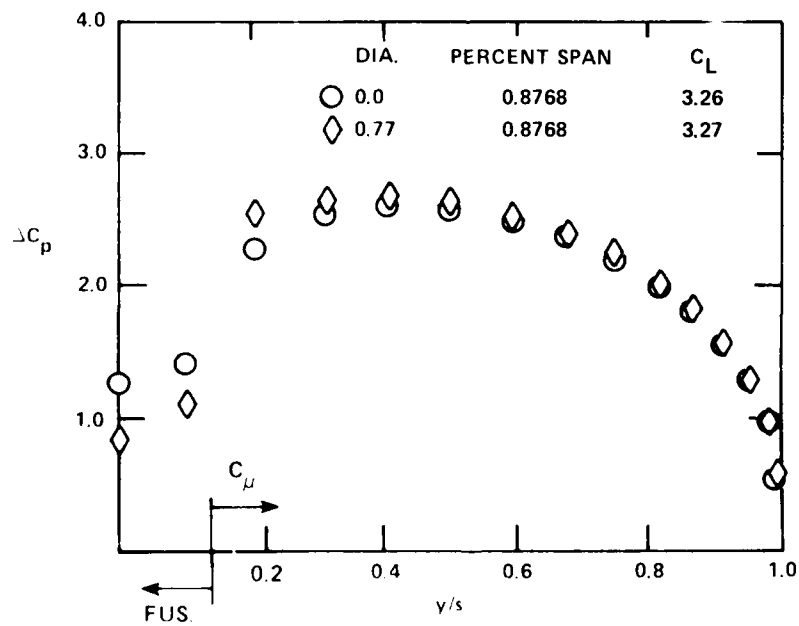Figure 5 – Spanwise Lift Distribution, $C_\mu = 0.0$

Figure 6 – Full Span Trailing Edge Blowing, $C_\mu = 0.1$, $\alpha = 3$ Degrees
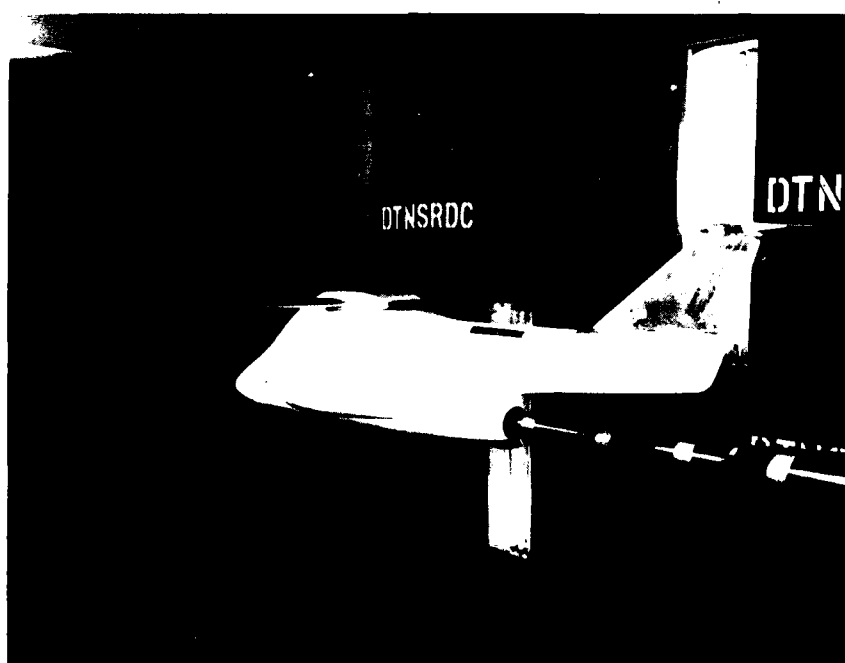
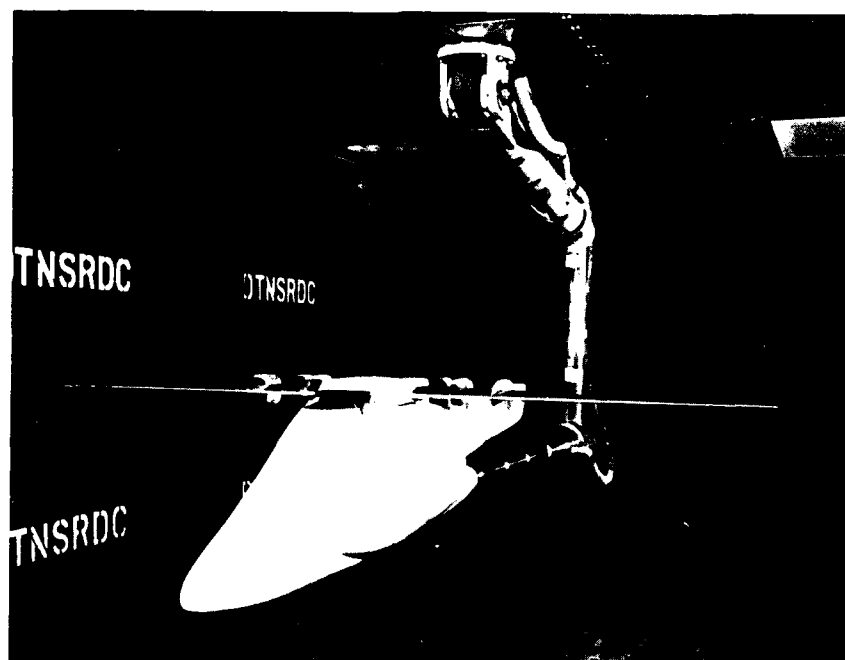Figure 4 - Model Installation in Subsonic Tunnel

13

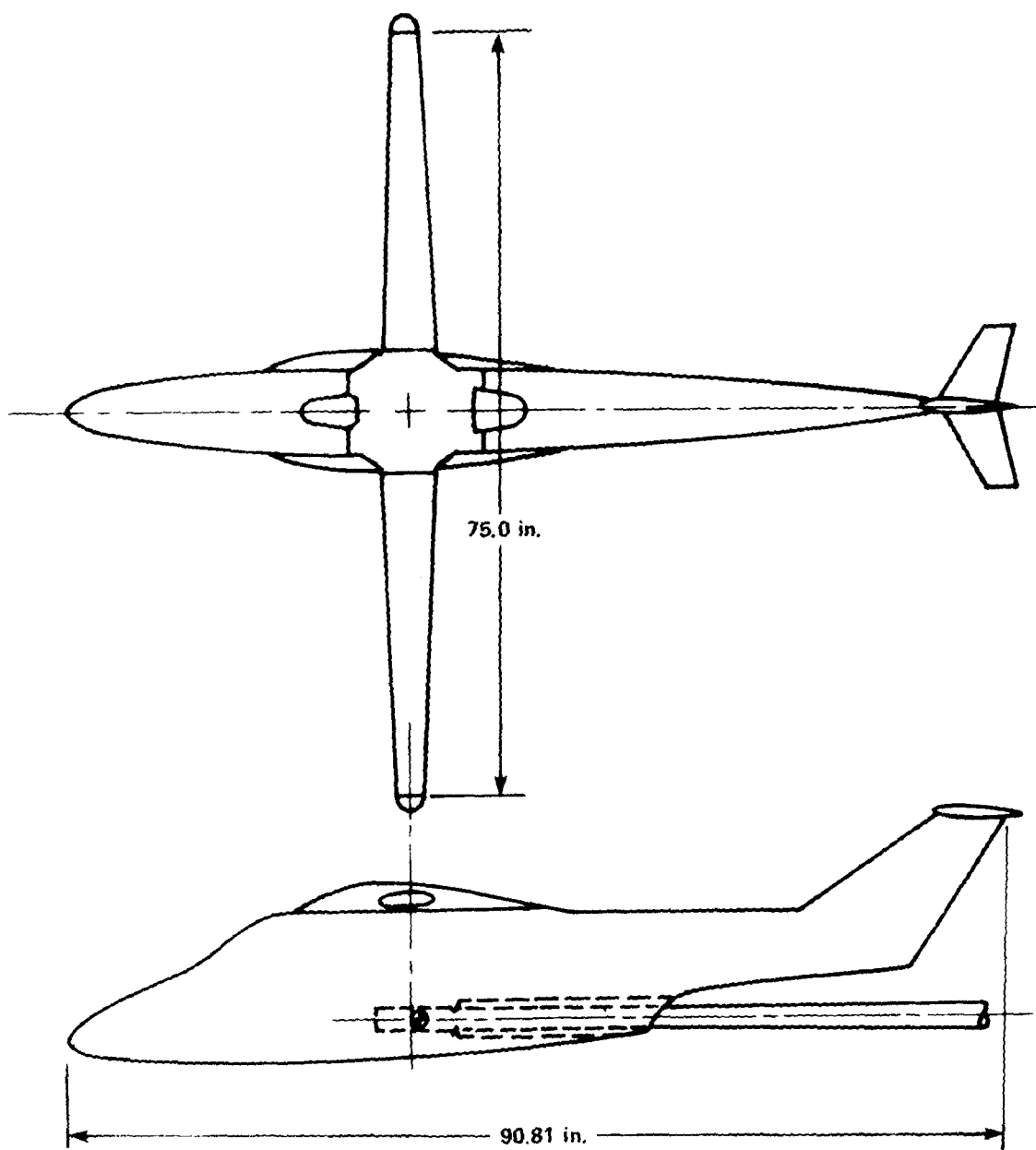Figure 3 — High Aspect Ratio Model

75.0 in.

90.81 in.
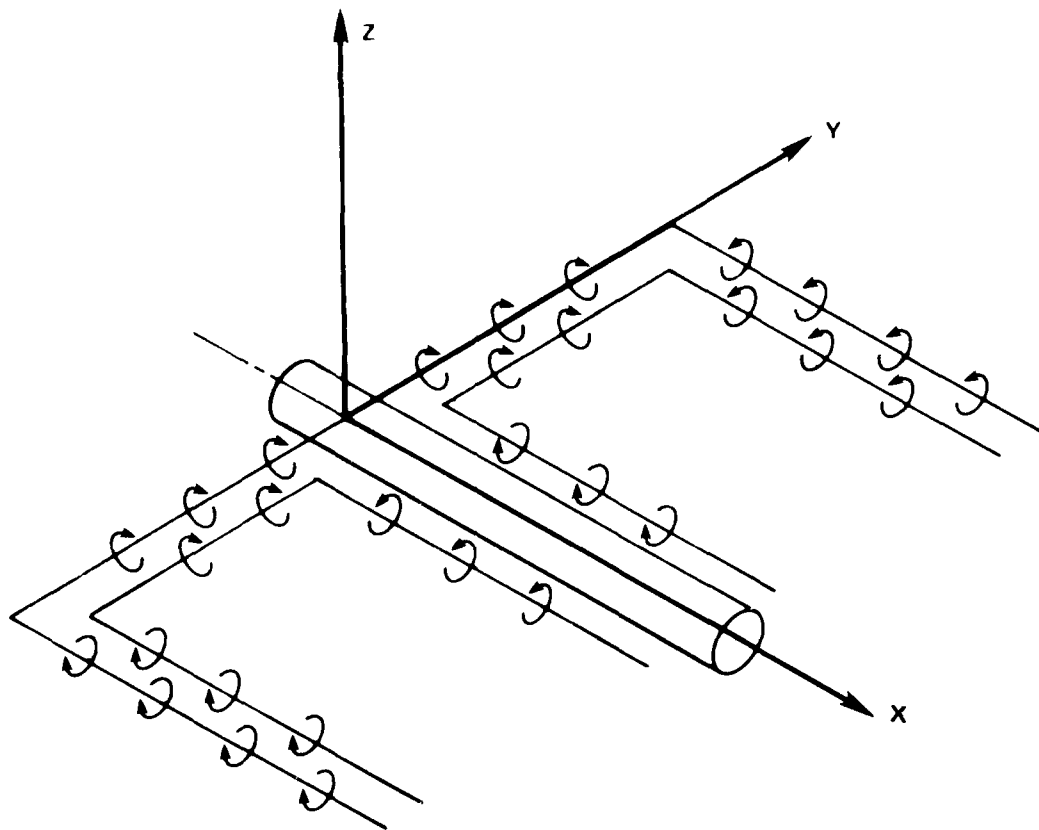
Figure 1 – Vortex Pattern for Circulation Control Wing/Body
Potential Flow Model

Figure 2 – Conventional Circulation Control Airfoil

The lift carried across the fuselage is found to decrease as the blowing portion of the span is moved outboard. The unblown segment of the wing, between the blowing portion and the fuselage, attains some benefit from the vortex pattern established by the blowing segment. The upwash generated in this region serves to increase the lift carried by this portion of the wing.

the trailing edge jet, this separation over the unblown section may be more extensive. Figure 25 shows the pressure coefficient a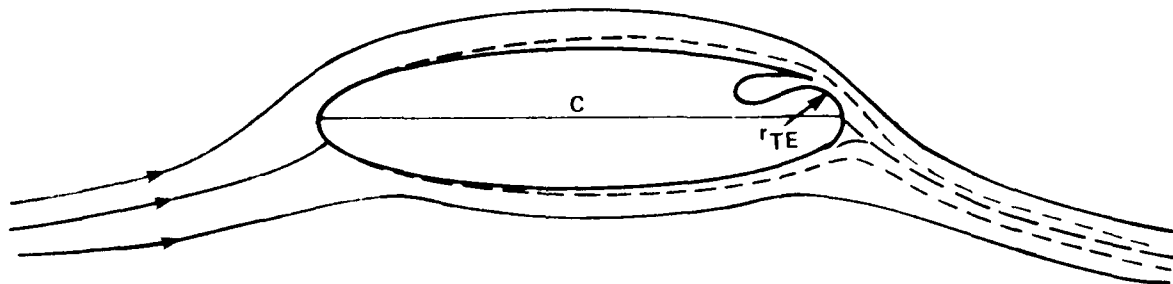s measured near the leading edge and mid-chord at the 20 percent span station of configuration 3. The pressure is shown to make a consistent change with increasing C_μ up to C_μ = 0.18. The next increase in C_μ does not show an appropriate change in pressure. Since this discrepancy occurs in the range of C_μ where it has already been stated that the circulation may not be enhanced with further blowing, the reason for the discrepancy is not clear. The fact that the pressure shows the flow to be still accelerating over the leading edge and decelerating toward midchord suggests that there is not extensive separation but rather the entire flow is not being augmented by the final increment in C_μ. This conclusion is borne out by the force data of Figure 21 which show the lift for C_μ = 0.237 to be less than that for C_μ = 0.18. Below C_μ = 0.15 the mathematical model and the data show good agreement and the fact that, while the fuselage carries less lift as the blowing moves outboard, the lift of the unblown portion of the wing is being enhanced by its proximity to the blown span.

Figures 26 through 29 show the process to repeat itself for configuration 4. The blowing portion of the wing is now restricted to the outer 67 percent of the span. The lift carryover across the fuselage is less than the previous configurations. The unblown segment of the wing again retains some benefit through the upwash generated by the blowing segment. The discrepancy shown in the lift distribution at the highest blowing rate, C_μ = 0.2, is again shown to coincide with the loss of augmentation apparent in the force data of Figure 26 for this C_μ.

CONCLUSIONS

A numerical model incorporating lifting line theory and a trailing edge vortex (to represent the lift augmentation produced by a trailing edge Coanda jet) is found to produce good correlation with experiment through moderate levels of trailing edge blowing. Spanwise lift distribution and lift coefficients show good agreement for blowing coefficients through approximately C_μ = 0.15. The good correlation is maintained as the percent of span with blowing is decreased.

Discrepancies between theory and experiment at the higher levels of C_μ are first attributable to leading edge flow separation on the wing itself and eventually to a loss of further augmentation through blowing.

0.21 and 0.27, the leading edge pressure increment shows inconsistent change with angle of attack, in particular at the 40 and 70 percent span stations, as would be expected in a region of separated flow. It appears that a leading edge separation bubble has formed at the higher blowing coefficients. In addition, the lack of an increase in the pressure difference between $C_\mu = 0.21$ and $C_\mu = 0.27$ is indicative that the overall circulation is not being increased, which is in agreement with the force data as noted in connection with Figure 11.

Figures 15 and 16 with $C_\mu = 0.1$ and 0.15, respectively, show agreement at what appears to be the upper limit of applicability for the potential flow model. The limit being the result of leading edge flow separation and a loss of further augmentation, through trailing edge blowing, in the real flow. The lift lost across the fuselage is also more accurately represented at the lowest blowing coefficients.

Figures 17 through 20 show lift coefficient data and typical pressure distributions for configuration 2. The wind tunnel model, and likewise the numerical model, have been modified to provide trailing edge blowing on the outer 82 percent of the span. The force data of Figure 17 show reasonable agreement with the lift and lift curve slope of the mathematical model up to a C_μ of 0.14. The lift distribution of the low to moderate blowing rates, Figures 8, 18, and 19, also show good agreement. Figure 20, with $C_\mu = 0.2$, shows considerable discrepancy between theory and experiment, again particularly at midspan of the blowing segment. For reasons as stated, the potential flow model for configuration 1 appears to have an upper limit near $C_\mu = 0.15$.

Figures 21 through 25 provide the lift and lift distribution for configuration 3. The blowing portion of the wing is now reduced to the outer 77 percent of the span. The lift and lift distribution are in good agreement again up to a C_μ near 0.15.

The section of the wing between the fuselage and the blowing segment is now approximately 10 percent of the span. While the agreement between theory and data is reasonable in this area as well, it does rate some special consideration. The given experiment that the blown portion of the span creates a local increase in incidence in this unblown area, at least for moderate levels of blowing. However, this portion of the wing does not have the favorable boundary layer control effect that exist on the blown segment. While a leading edge separation may occur on the blown portion of the wing, but reattach due to the boundary layer control effect of

8

disagreement shows at the higher C_μ levels. This could be a result of the math. model exceeding the range of its inherent small angle assumptions or, as the data indicate, the model may be experiencing some flow separation. Flow separation with its resultant loss of lift may show itself here in two forms: first through the loss of lift with increasing α for a given C_μ, and second with that lost (or not gained) with a given α and increasing C_μ. In the first case, this would be attributable to local flow separation on the airfoil surface itself. In the second instance, flow separation may not occur on the airfoil itself, but rather the Coanda jet detaches closer to the slot and thereby shows a reduction in the induced circulation. This effect may be associated with the jet velocity reaching sonic conditions and the resulting expansion-contraction waves adding to the adverse pressure gradient seen by the jet, and causing earlier jet detachment from the Coanda surface.

The solid data of Figure 11 provide a good example of the two types of separation. The data for $C_\mu = 0.15$ show the first signs of flow separation when going from $\alpha = 0$ deg to $\alpha = 3$ deg. This would be consistent with local flow separation on the airfoil surface itself. The data for $C_\mu = 0.27$ show its lift coefficient to be less than that for the next lowest value of C_μ for the entire angle-of-attack range. This would suggest that the induced circulation is no longer being enhanced and that the noted sonic jet velocity implies that the second type of separation has occurred. At $C_\mu = 0.27$ and $\alpha = 3$ deg it appears that both types have occurred.

The lift distribution for a moderate level of C_μ is provided in Figure 12. Good corroboration is seen in both distribution and lift coefficient. Figure 13 shows a comparison at $C_\mu = 0.21$. The level of trailing edge blowing here is above that where some flow separation is indicated in the data of Figure 11. The disagreement in the lift distribution is seen to be greatest at the 40 and 70 percent span stations, that is, where the local effective incidence would be at its largest. Further evidence of surface separation is provided by the chordwise experimental pressure distribution, as measured near the leading edge and midchord, shown in Figure 14. The data are for the C_μ values of 0.05, 0.21, and 0.27 and are shown for the spanwise stations of 20, 40, 70, and 90 percent span. Each plot covers a range in α of approximately -3.0 to +3.0 deg. The incremental rise in the leading edge pressure coefficient with α at the moderate $C_\mu = 0.0498$ is seen to be consistent at the four spanwise stations shown in Figures 14a through 14d. At the higher blowing momentum coefficients of

blowing; configuration 1, with full trailing edge blowing from wing root to tip through configuration 4 with blowing on the outer 67 percent of the span. The spanwise extent of the trailing edge blowing is indicated on the figures. The correlation between theory and experiments, at these moderate blowing momentum coefficients, is good in all four cases for both lift distribution and total lift coefficient.

An interesting feature of the mathematical model is shown in the lift distribution of configurations 2 through 4. As indicated in the vortex pattern of Figure 1, an upwash, emanating from the blown portion of the span, between the inboard terminus of the blown span and the fuselage, can be expected. A measure of this upwash is provided by extending the application of Equation (A.1) into the unblown region of the wing. While α'_{cc} is zero in this region, α_{icc} is not and is provided by Equation (A.9). The flow in this region is further complicated by the presence of the fuselage. The lift carried by the fuselage is seen to decrease as the blowing segment moves outboard, away from the fuselage. This is attributed to a reduction in the upwash at the fuselage as the blowing moves outboard and is accurately simulated by the mathematical model. The upwash in this region of the wing should also contribute to an increase in the local effective incidence. This likewise shows itself in the data and model on configurations 3 and 4 (Figures 9 and 10) between the fuselage and the blowing segment.

The form of the lifting line solution provides for a less dense distribution of calculated points, for a given N, on the inboard portion of the wing. While a greater computer capacity than was used in the development of this model would provide more clarity in this region, the correlation shown in Figures 7 through 10 is good.

Figure 11 shows the lift coefficient for configuration 1 as a function of α and C_μ. The discrepancy shown between theory and experiment for the no-blowing case can be attributed to the wing camber and trailing edge bluntness. The inviscid theoretical model will respond to the wing camber and show some lift at zero alpha. The wind tunnel model, without trailing edge blowing, will develop some flow separation at the blunt trailing edge and thereby will not fully respond to the wing camber. The difference in lift at zero alpha is maintained through the angle-of-attack range with the result that the lift curve slope is in good agreement. The figure shows good agreement between theory and practice at moderate C_μ levels. Gradual

6

with pressure taps. The test program provided pressure data through the range -3 deg $\leq \alpha \leq + 3.0$ deg. Force data were obtained from $\alpha = -3$ deg through stall, and for the blowing momentum coefficient range, $0.0 \leq C_\mu \leq 0.3$. Test conditions provided for a free-stream dynamic pressure of 30 lb/ft^2 and a unit Reynolds number of 1.0×10^6.

The details of the test procedure and resulting force and pressure data are described by Jacobsen.* Only that pertinent to correlating with the present mathematical model and determining the lift carryover on the fuselage will be used here.

RESULTS AND DISCUSSION

The fuselage effect on the spanwise lift distribution of a tapered, high-aspect ratio wing, with no trailing edge blowing, is shown in Figure 5. The experimental lift distribution in this and succeeding figures is, in fact, the difference in upper and lower surface pressure coefficient at the 50 percent chord position,

$$\Delta C_{p_{0.5c}} = \left(C_{p_\ell} - C_{p_u} \right)_{0.5c}$$

as this provides for a convenient comparison with the numerical results provided by Equation (A.16). The numerical results show the same total lift for the isolated wing as for the wing-body combination. The presence of the body is seen to alter the distribution such that the lift lost over the fuselage itself is regained on the inboard section of the wing as a result of a local angle of attack increase produced by the body. This is in keeping with known results (Reference 1). The effect of including the trailing edge blowing is shown in Figure 6. In a similar manner to the no blowing case, the lift lost over the fuselage is regained near the wing root such that the total lift is unchanged. The large drop in the local lift, with or without the fuselage present, is attributed to the vortex system being induced by the limited spanwise trailing edge blowing.

Figures 7 through 10 provide a comparison of the theoretical model with experiment for moderate blowing and for each of the four configurations comprising the test sequence. Configurations 1 through 4 provide a decreasing percent of span

_____

*As indicated by Jacobsen in a DTNSRDC informal report, "Wind Tunnel Investigation of a High Aspect Ratio Circulation Control Wing," of Jul 1983.

$$\sum_{n=1}^{\infty} A_n \sin n\theta \ \{n\mu[1+f(y)] + \sin \theta\} = \mu \ (\alpha_g + \alpha_c + \alpha_{cc}) \sin \theta \qquad (7)$$

where

$$\mu = \frac{a_o c}{4b} \qquad (8)$$

with $c = c_r [1-(1-\lambda) \cos \theta]$ providing for wing taper.

Equation (7) provides a series of simultaneous equations, the solution of which leads to the desired spanwise lift distribution. With the exception of the circulation or blowing induced incidence, α_{cc}, the remaining input variables for Equation (7) are provided by the fuselage and wing geometry. The procedure for determining the blowing induced incidence and development of the complete wing-body model is provided in the appendix.

EXPERIMENTAL PROGRAM

The high aspect ratio circulation control wing data were provided by an experimental program carried out in the DTNSRDC 8- by 10-ft subsonic wind tunnel. The model, shown both schematically in Figure 3 and installed in the tunnel in Figure 4, has a 75-in. wing span with an aspect ratio of 18 and taper ratio of 0.5. The elliptic shaped airfoil has a thickness ratio of 0.20 at the root and 0.15 at the tip. The ratio of the trailing edge radius to the chord varied from 5.3 percent at the root section to 2.2 percent at the tip. The wing, shown in planform in Figure 3, has a trailing edge slot forming the Coanda jet, running the entire span. In order to better determine the lift carryover, or pressure effects spanwise across the fuselage, the jet flow was restricted from the root section outboard to form four configurations. The exposed slot-to-span ratio was 0.877, 0.8249, 0.7744, and 0.675 (corresponding respectively to configurations 1 through 4). (Actually, the full span up to fuselage attained the value 0.877 when considering the full span as extending to the fuselage centerline.) The wing has 5 percent camber at the root and tapers to no camber at the tip. Detailed wing characteristics are provided in Table 1. The fuselage (faired to the wing at the wing station) and wing were extensively instrumented
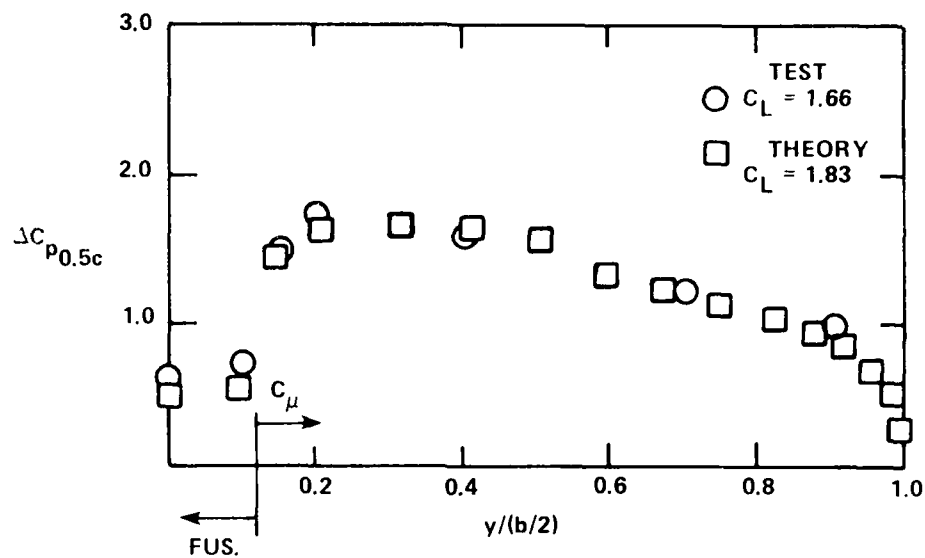
4

Figure 12 – Spanwise Distribution, Configuration 1,
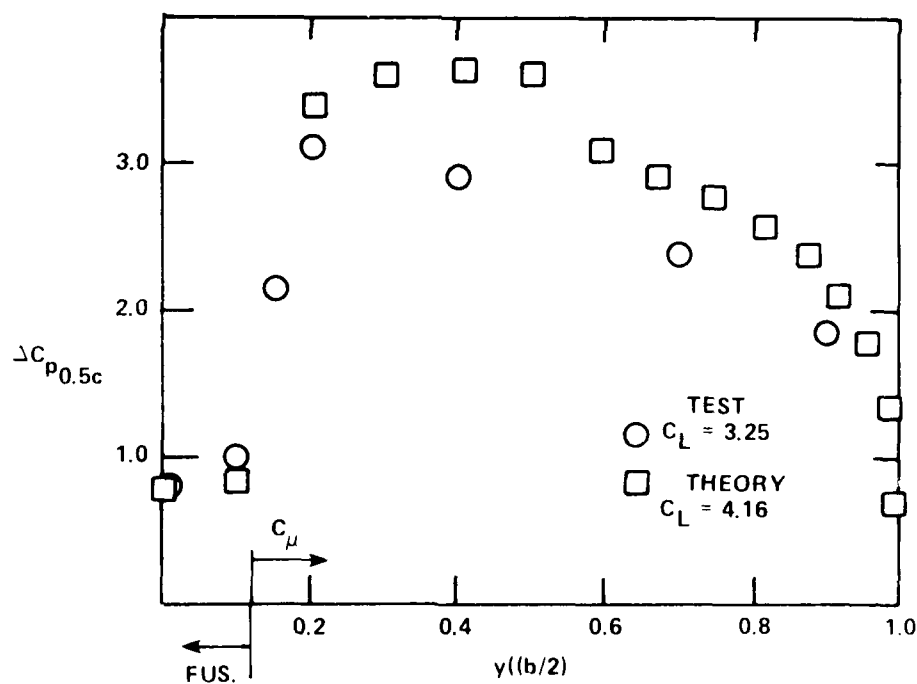$C_\mu = 0.0496$, $\alpha = 0.20$ Degrees

Figure 13 – Spanwise Distribution, Configuration 1,
$C_\mu = 0.211$, $\alpha = 3.6$ Degrees

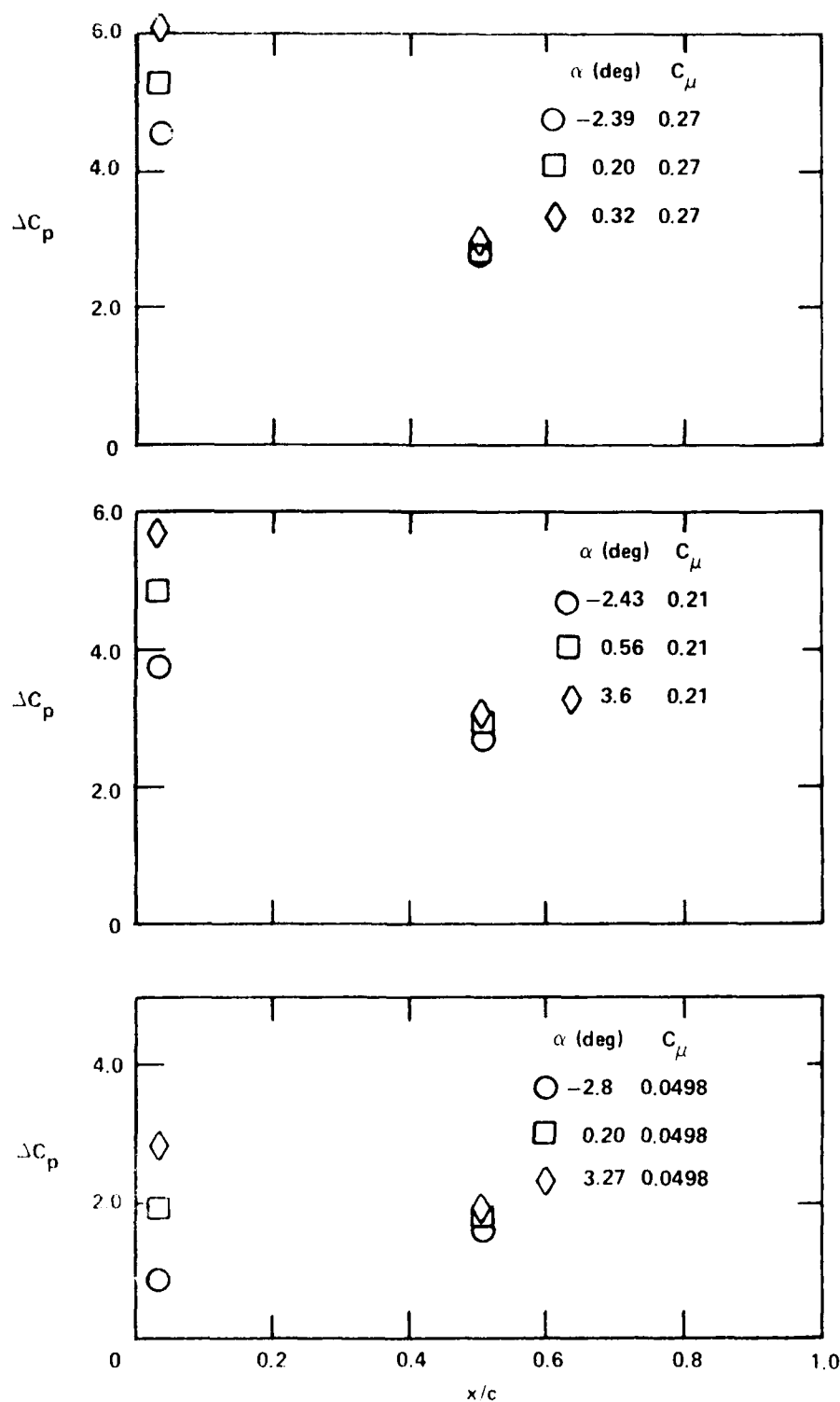Figure 14 – Experimental Chordwise Pressure Distribution,
Configuration 1

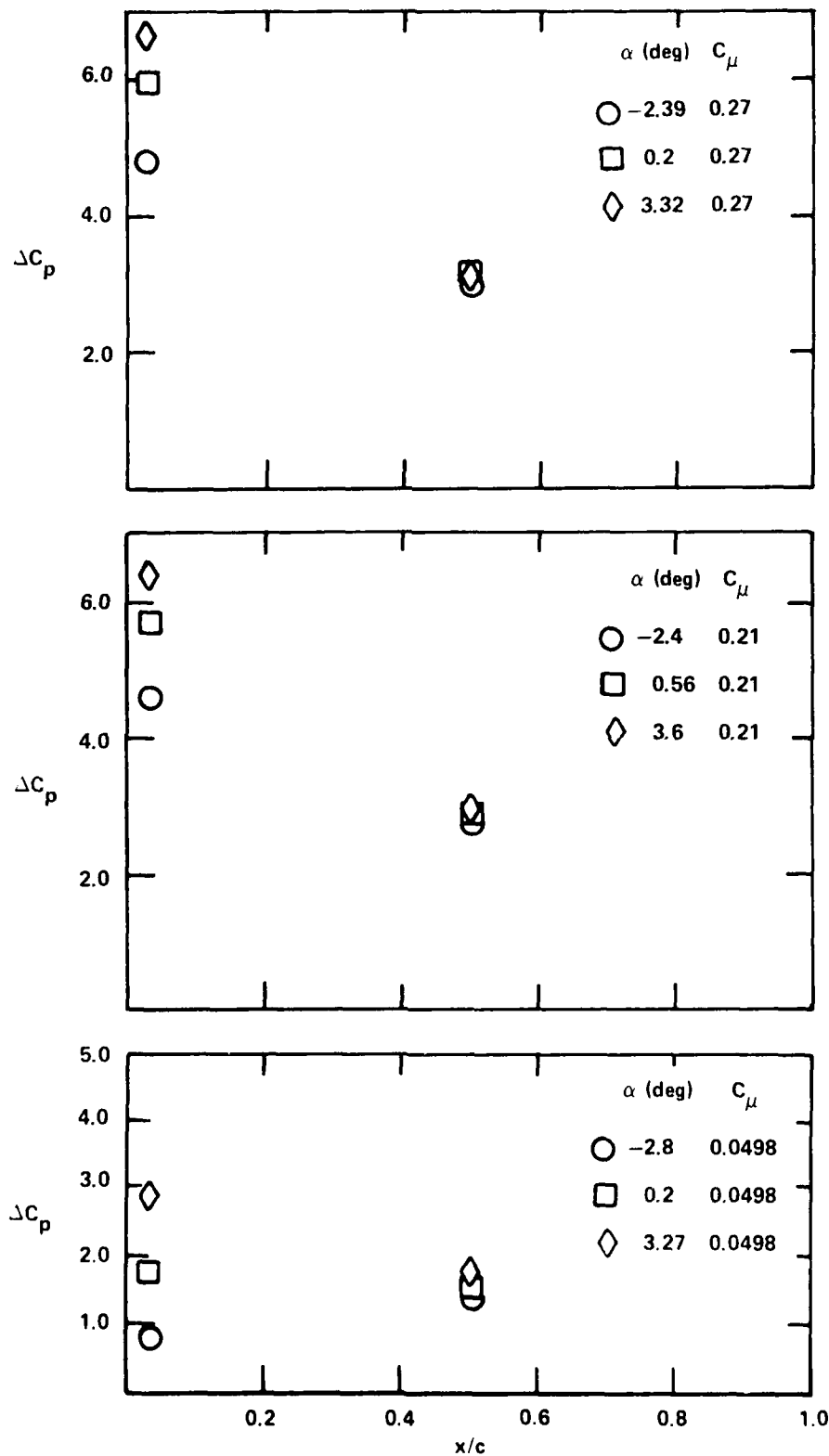Figure 14a – 20 Percent Span

19

Figure 14 (Continued)

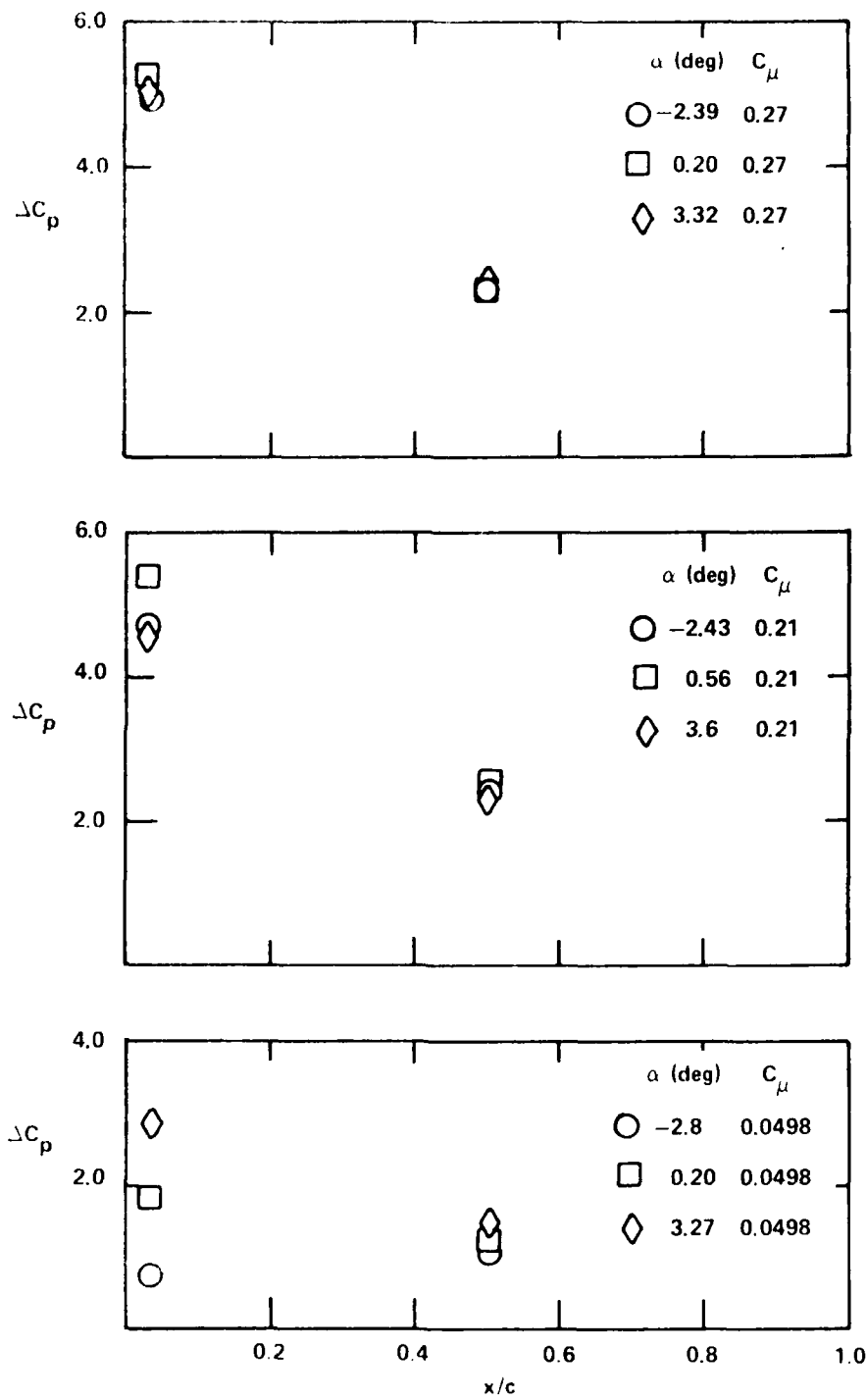Figure 14b - 40 Percent Span

20

Figure 14 (Continued)
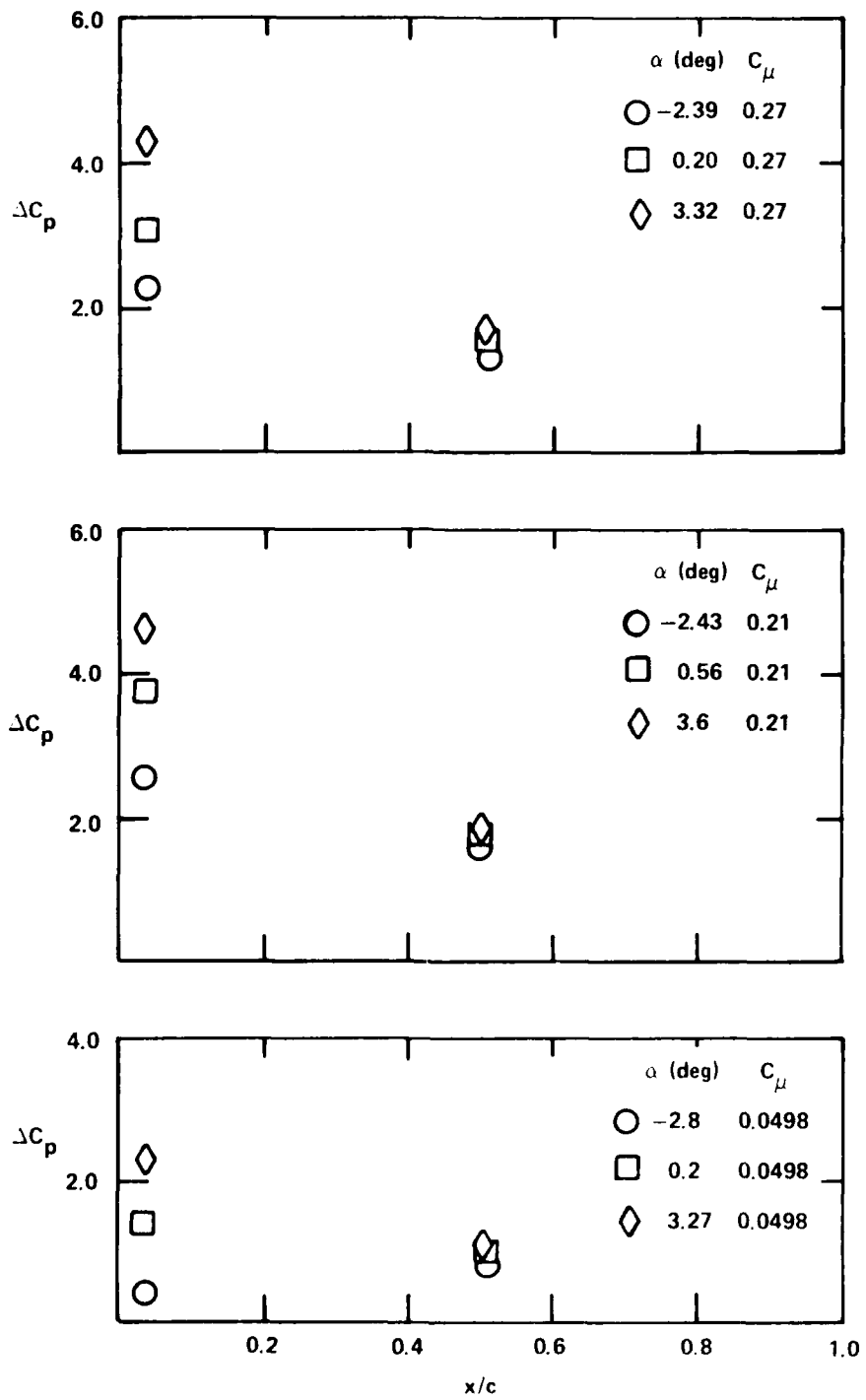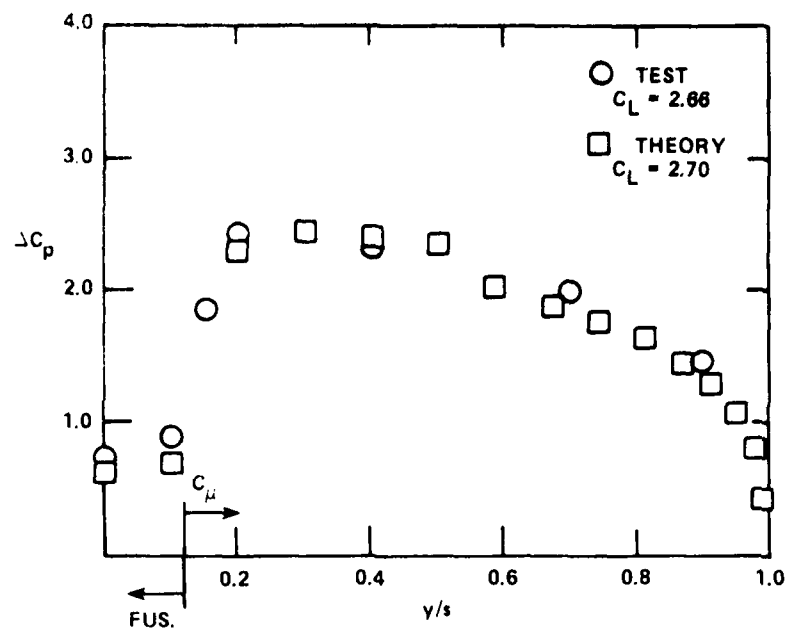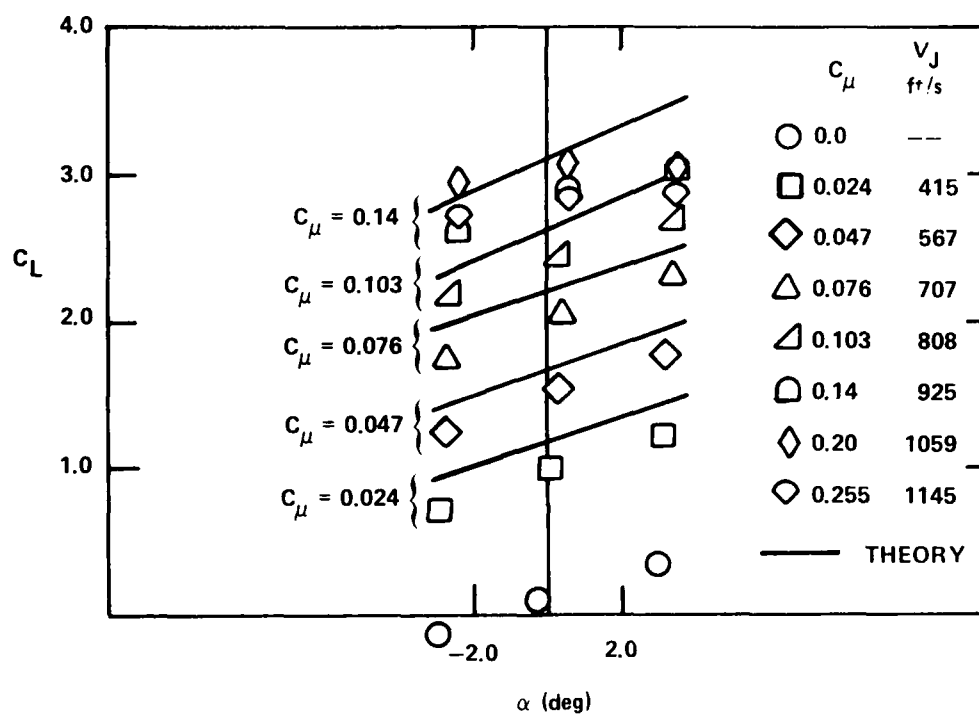

Figure 14c – 70 Percent Span

21

Figure 14 (Continued)

Figure 14d - 90 Percent Span

22
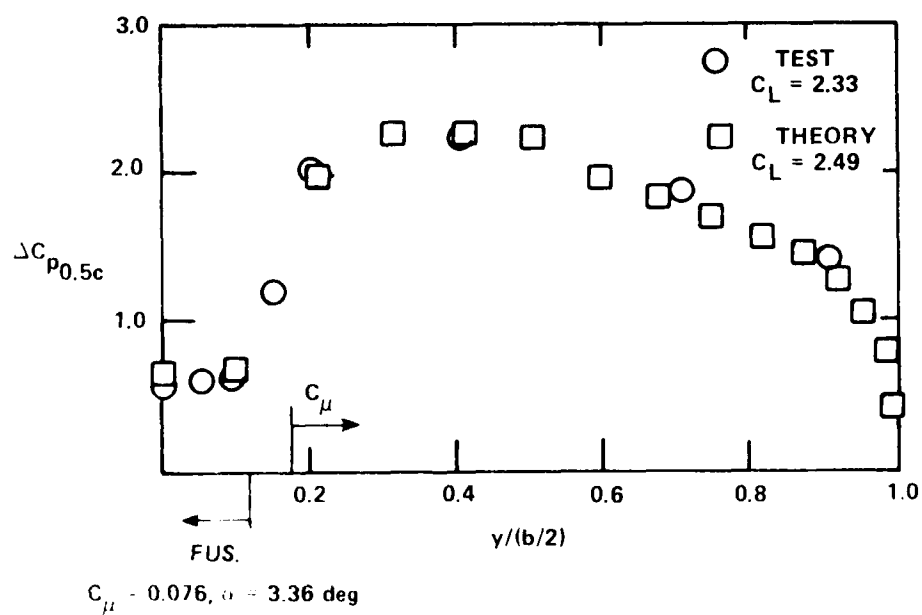
Figure 15 - Span Lift Distribution, Configuration 1,
$C_\mu = 0.1076$, $\alpha = 0.44$ Degrees
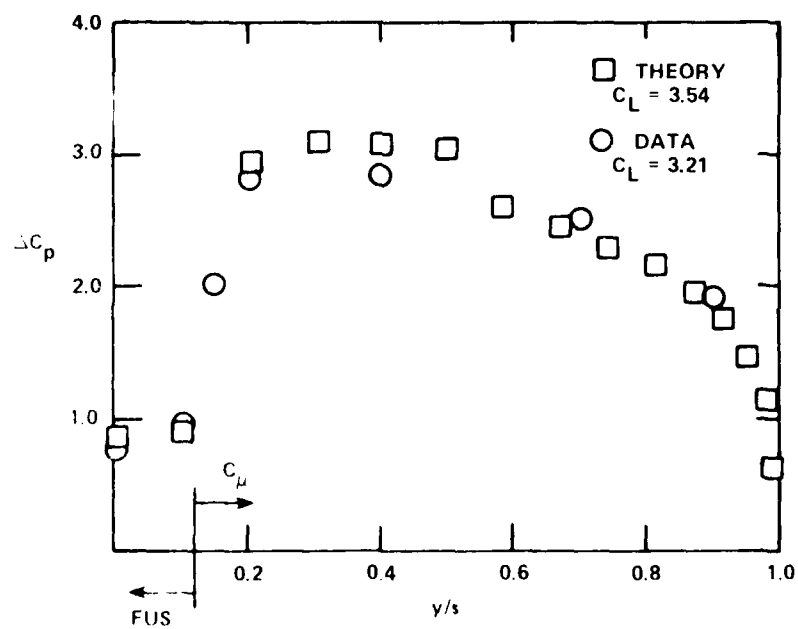
Figure 16 - Span Lift Distribution, Configuration 1,
$C_\mu = 0.1474$, $\alpha = 3.5$ Degrees

23

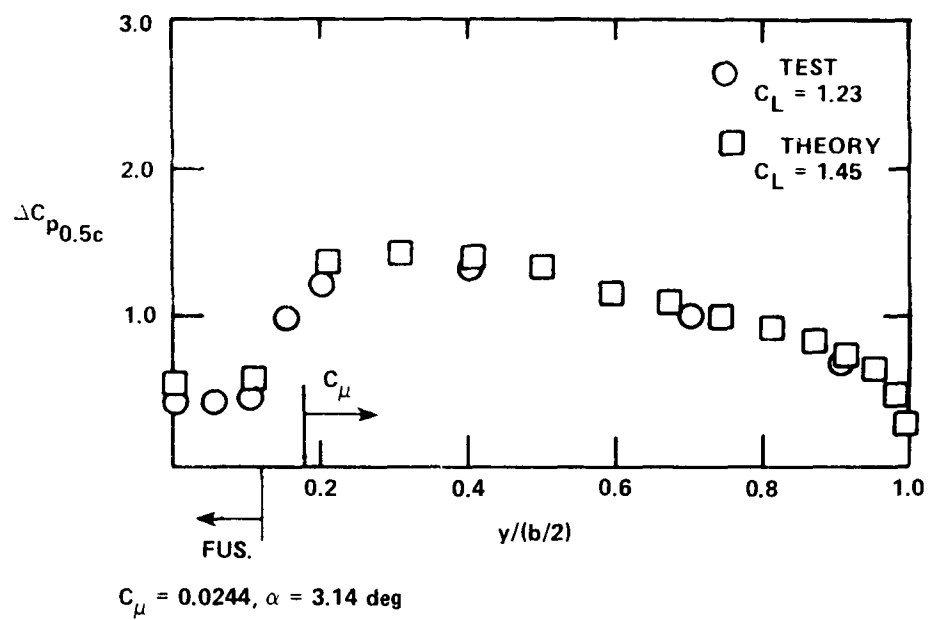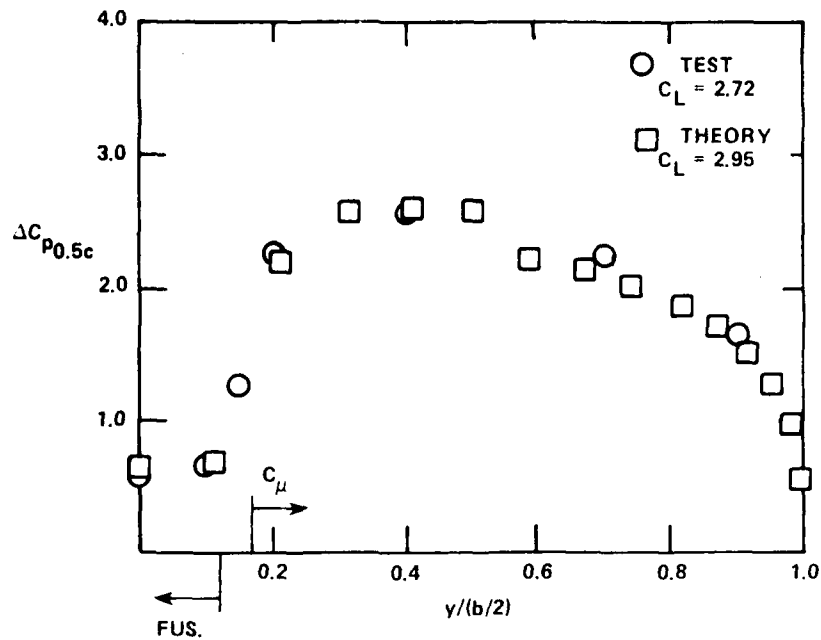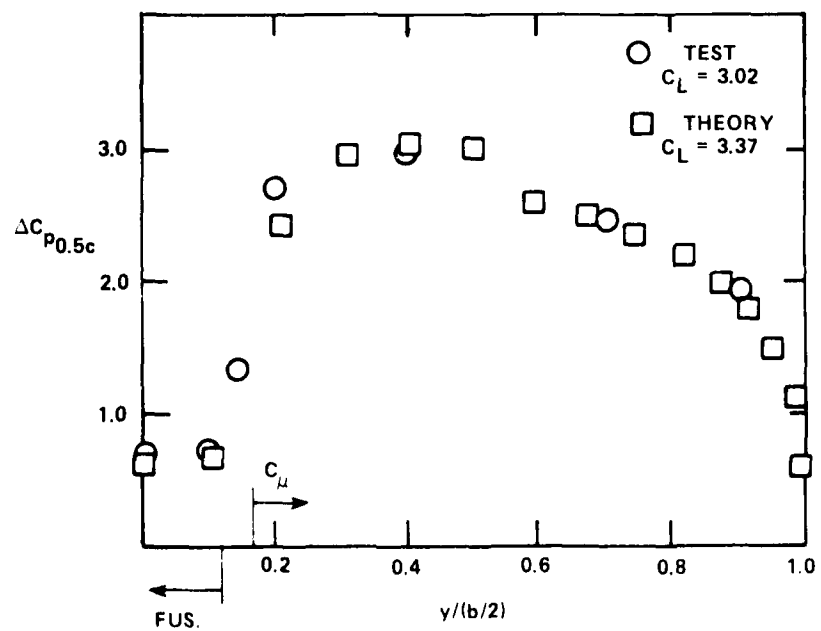Figure 17 – Lift Coefficient, Force Data and Theory,
Configuration 2

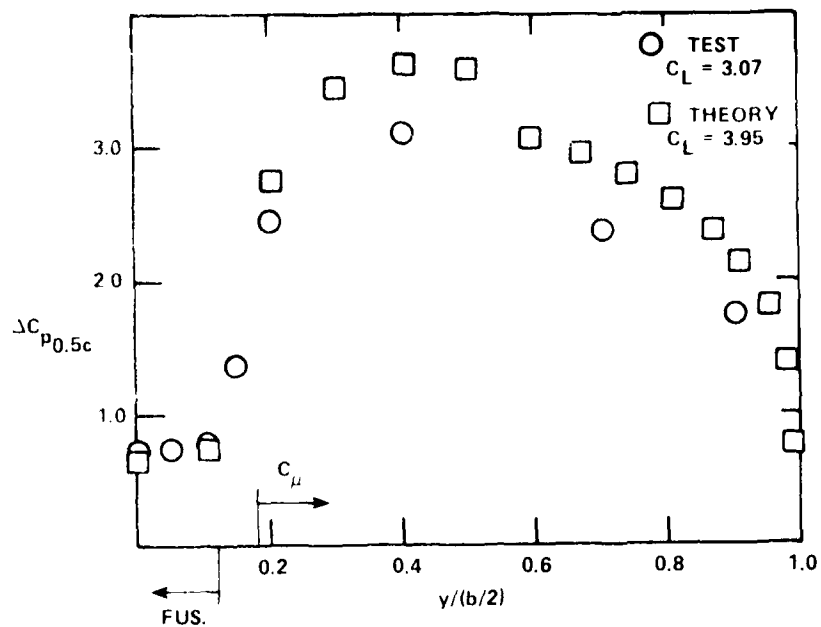Figure 18 - Span Lift Distribution, Configuration 2,
$C_\mu = 0.0244$ and 0.076

$C_\mu = 0.1026$, $\alpha = 3.42$ deg = 0.0597 rad

$C_\mu = 0.14$, $\alpha = 3.5$ deg = 0.061 rad

Figure 19 – Span Lift Distribution, Configuration 2, $C_\mu = 0.1026$ and 0.14

Figure 20 - Span Lift Distribution, Configuration 2,
$C_\mu = 0.202$

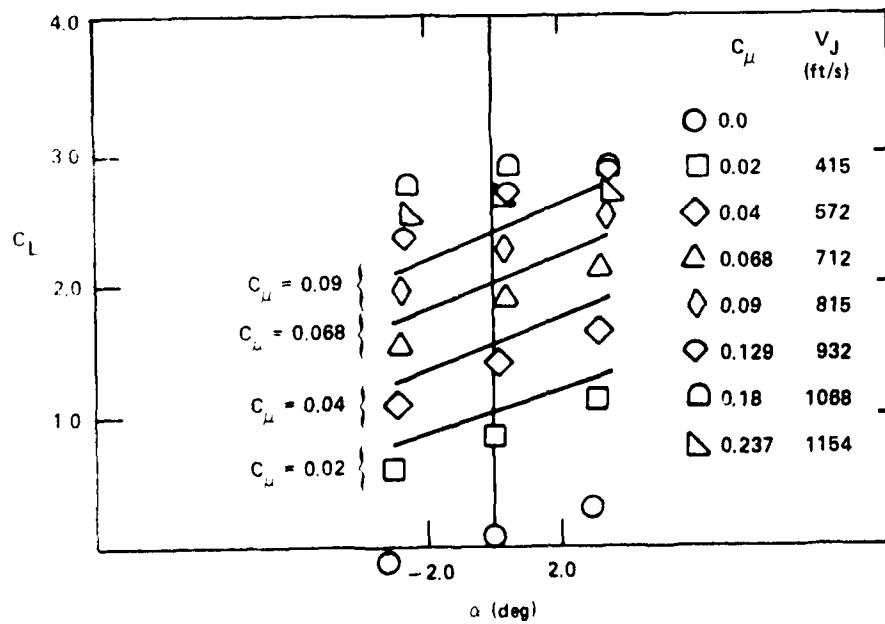$C_\mu = 0.202$, $\alpha = 3.51$ deg = 0.0613 rad

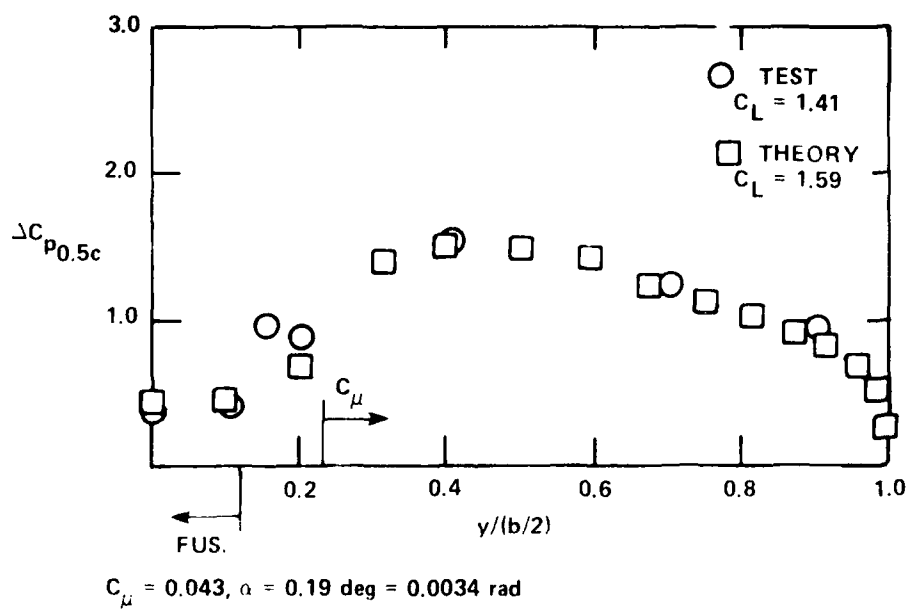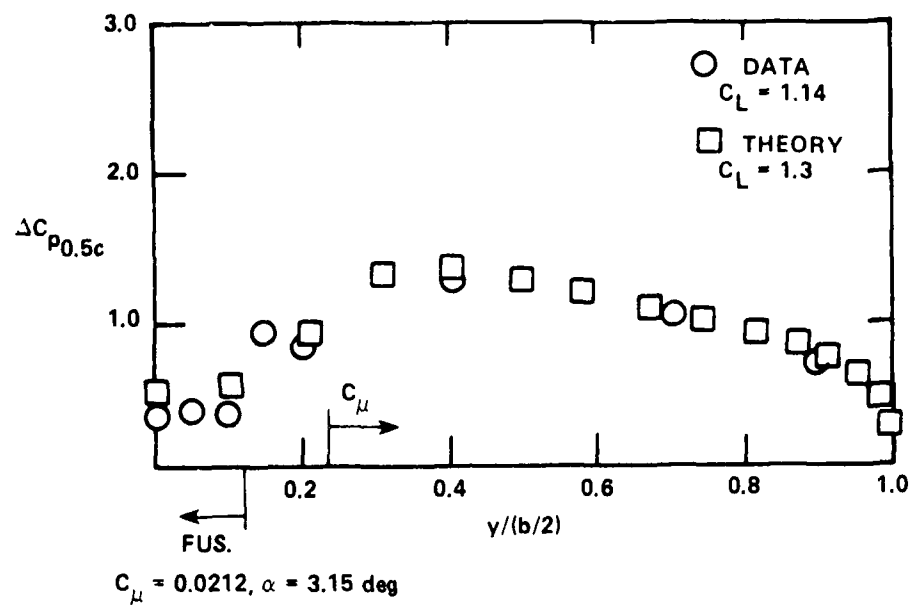Figure 21 - Lift Coefficient, Force Data and Theory,
Configuration 3
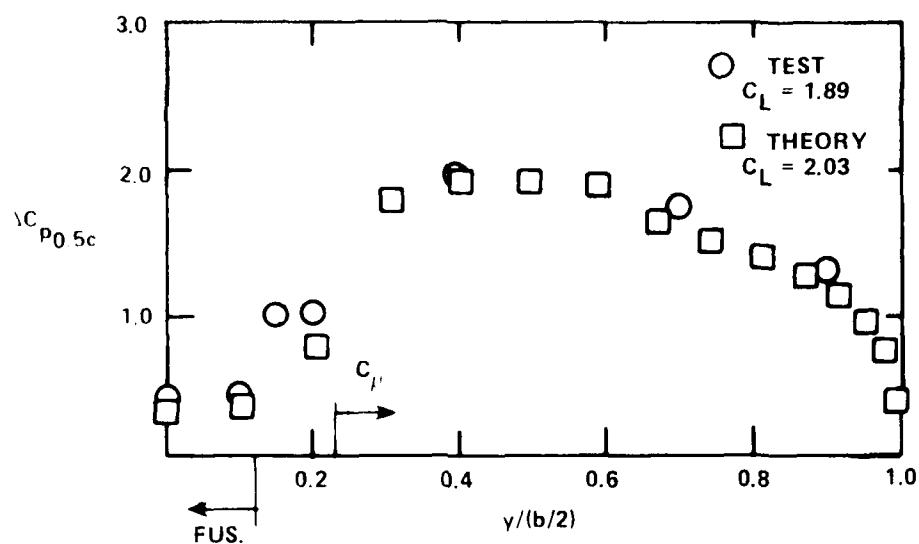
Figure 22 - Span Lift Distribution, Configuration 3,
$C_\mu = 0.0212$ and 0.043

$C_\mu = 0.0694$, $\alpha = 0.29$ deg

$C_\mu = 0.09$, $\alpha = 0.37$ deg
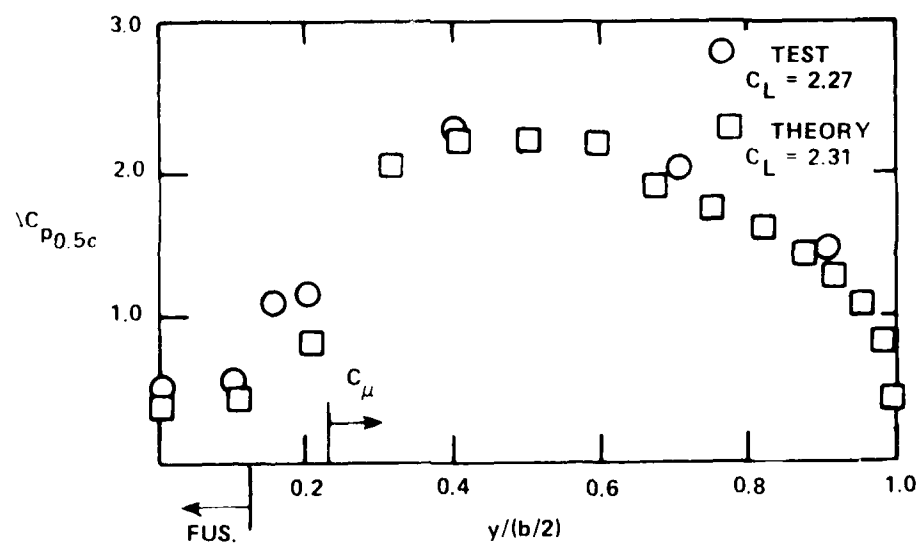
Figure 23 – Span Lift Distribution, Configuration 3, $C_\mu = 0.0694$ and 0.09

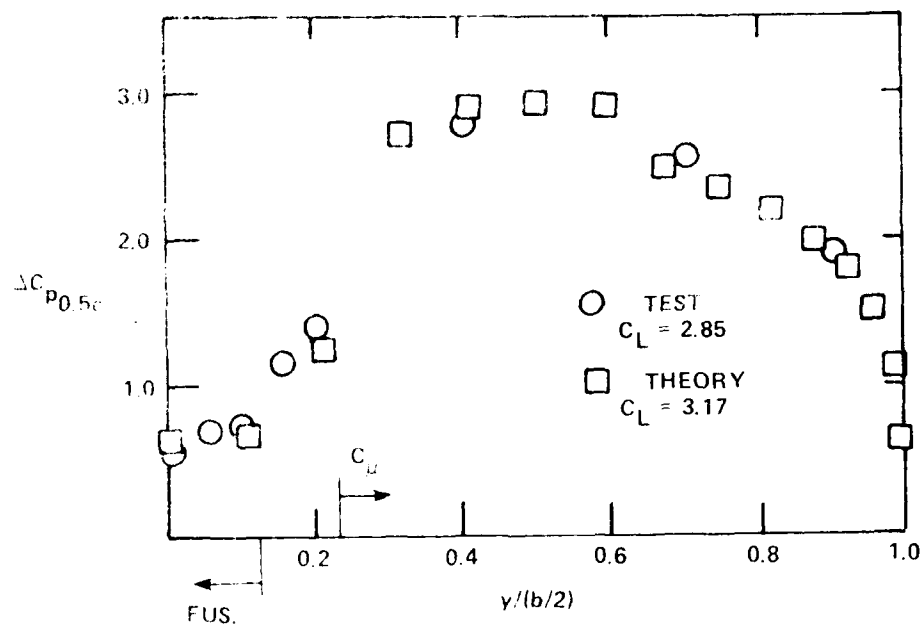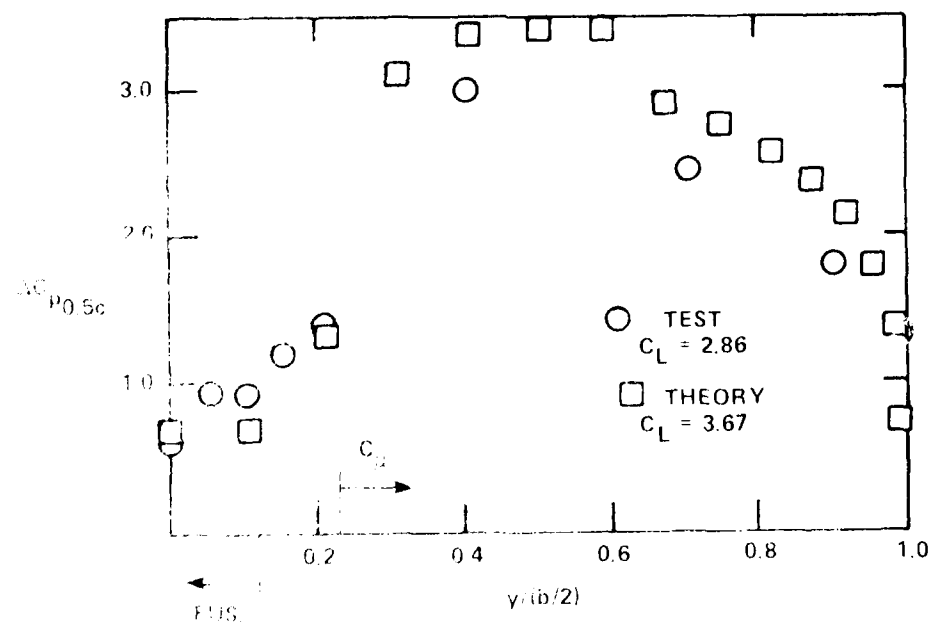$C_\mu = 0.13$, $\alpha = 3.48$ deg

$C_\mu = 0.18$, $\alpha = 3.48$ deg

Span Lift Distribution, Configuration 3,
$C_\mu = 0.13$ and 0.18
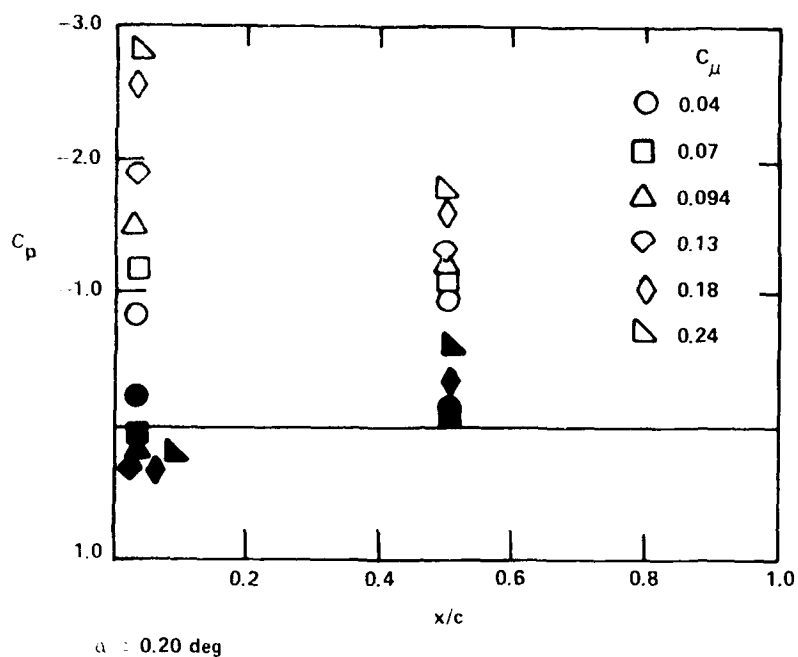
Figure 25 - Chordwise Pressure Distribution at Unblown Span
Station, Configuration 3 at 0.2 Semispan
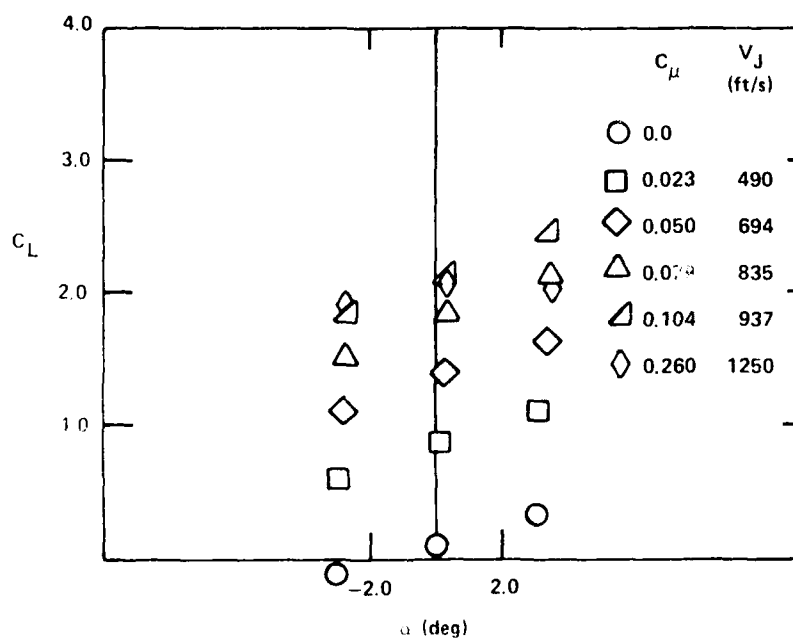
Figure 26 - Lift Coefficient, Configuration 4

McDonnell Douglas/Long Beach

Northrop Corp./Aircraft Div

Rockwell International/Columbus

Rockwell International/Los Angeles

U.S. Naval Aeronautical

CENTER DISTRIBUTION

Copies	Code	Name
	012.3	Research Coordinator
1	16	Dr. Chapman
1	166	R. Furey
1	166	Nichols
	166.4	Aerodynamics Collection
	5211.1	Reports Distribution
	522.1	TIC (C) +1m
		TIC (A)
		Patent Counsel

INITIAL DISTRIBUTION

Copies		Copies	
1	DARPA (AVTO)/COL Allburn	1	California Inst of Technology Aeronautics Lib
1	DIA/P. Scheurich	1	Cornell U/Tech Lib
1	CMC/Science Advisor	1	Ohio State U/O. Burgraff
1	CNR/R. Whitehead (Code 432)	1	Stanford U/N.J. Wood
2	NRL 1 Tech Lib 1 R. Foch	1	U of Kansas E. Lan/Aero Engr Dept
1	NAVMAT/CDR Fuller (0711)	1	U of Maryland/J. Anderson
1	NAVPGSCOL/Tech Lib	1	U of Southern California H.K. Cheng
4	NAVAIRDEVCEN 1 Tech Lib 1 6053/J. Clark 1 6053/C. Mazza 1 6053/M. Walters	1	U of West Va/Aero Engr Lib
		1	Analytical Methods, Inc. F. Dvorak
5	NAVAIRSYSCOM 1 AIR-7226/Tech Lib 1 AIR-03D/G. Heiche 1 AIR-310/T. Momiyama 1 AIR-310D/J. Durkin 1 AIR-5301/R. Tracy	1	Boeing Comm Airplane Co/Seattle 1 Tech Lib 1 W. Clay
		1	Douglas Aircraft Co/Tech Lib
12	DTIC	2	General Dynamics/Ft. Worth 1 Tech Lib 1 W. Foley
1	HQ, ASD/F. Krause (XRS)	2	Grumman Aerospace Corp 1 Tech Lib 1 M. Siegel
1	AFT/M. Franke		
1	AFOSR/Aero Sciences	1	Ling-Temco-Vought, Inc. Tech Lib
2	AFWAL 1 Tech Lib 1 FIMM	1	Lockheed California Co Tech Lib
2	NASA Ames Research Center 1 Tech Lib 1 G. Kidwell	3	Lockheed Georgia Co 1 Tech Lib 1 C. Dixon 1 W. English
2	NASA Langley Research Center 1 Tech Lib 1 L. Parlson (Code 236)		

REFERENCES

1. Thwaites, B., "Incompressible Aerodynamics," Oxford University Press (1960).

2. Maskell, E.C. and D.A. Spence, "A Theory of the Jet Flap in Three Dimensions," Proceedings Royal Society (1959).

3. Flax, A.H., "Integral Relations in the Linearized Theory of Wing-Body Interference," Journal of the Aeronautical Sciences, Vol. 20 (1953).

4. Spence, D.A., "The Lift Coefficient of a Thin, Jet-Flapped Wing," Proceedings Royal Society (1956).

5. Karamcheti, K., "Principles of Ideal-Fluid Aerodynamics," Robert E. Krieger Publishing Co., Inc. (1980).

6. Smith, R.V. et al., "Discrete Vortex Modeling Applied to the Prediction of Circulation Control," Journal of Fluid Mechanics (1980).

7. Wood, N.J., "The Aerodynamics of Circulation Control Aerofoils," Stanford University Report JIAA-41 (Jul 1981).

For any large aspect ratio wing, the lift distribution can be related to that of a flat plate in the form:[1]

$$\ell(x,y) = \frac{\Delta p}{q_\infty} = \frac{2}{\pi} C_L(y) \left[\frac{x_T(y) - x}{x - x_L(y)} \right]^{1/2}$$

For the midchord position this reduces to:

$$\ell(y)_{0.5c} = \Delta C_{P_{0.5c}} = \frac{2}{\pi} C_L(y) \tag{A.16}$$

which provides for convenient comparison with the experimental data.

The overall lift coefficient is provided by:

$$\bar{C}_L = \frac{1}{\bar{c}b} \int_{-\frac{b}{2}}^{\frac{b}{2}} C_L(y) \, c(y) \, dy$$

A computer program utilizing this mathematical model was written and applied to correlate with the data from the experimental model.

This can be treated in a similar manner to that of (A.7) with additional considerations for the presence of the body. The cross flow induced by the presence of the body when the wing and body are at the same incidence is:

$$\alpha(y) + \alpha(y) \ f(y) = \alpha_e(y) + \alpha_i(y) \tag{A.11}$$

for $y \geq d/2$, where $\alpha(y)$ includes the effects of geometric and camber induced incidence. For a circular arc imposed camber,

$$\alpha_c = 2 \times camber$$

In obtaining the coefficients A_n the downwash distribution and α_i can be determined through Equation (4).

In keeping with the initially stated concept of the mathematical model, the local total lift coefficient is then provided by:

$$C_{L_T} = \left(\frac{\partial C_L}{\partial \alpha}\right)_{\alpha=0} (\alpha_g + \alpha_c + \alpha_{cc} - \alpha_i) + \left(\frac{\partial C_L}{\partial \alpha_{cc}}\right) \alpha_{cc} \tag{A.12}$$

where the empirically derived values of Spence:[4]

$$\left(\frac{\partial C_L}{\partial \alpha}\right)_{\alpha=0} = 2\pi \left(1 + \frac{t}{c}\right) (1 + 0.151 \ C_\mu^{1/2} + 0.219 \ C_\mu) \tag{A.13}$$

$$\frac{\partial C_L}{\partial \alpha_{cc}} = 2(\pi C_\mu)^{1/2} (1 + 0.151 \ C_\mu^{1/2} + 0.139 \ C_\mu)^{1/2} \tag{A.14}$$

are applied locally. Inboard of the wing body juncture the lift coefficient is provided, in accordance with Thwaites,[1] as:

$$C_{L_T}(y) \Big|_{y < \frac{d}{2}} = C_{L_J} - \frac{4}{c_J} \ w_J \ (d^2 - 4y^2)^{1/2} \tag{A.15}$$

41

in the range

$$-\frac{b_{cc}}{2} \leq y_{cc} \leq \frac{b_{cc}}{2}$$

The empirically derived form of Maskell and Spence[2] provides a_o.

$$a_o = \left(\frac{\partial C_L}{\partial \alpha}\right)_{\alpha=0} = 2\pi \left(1 + \frac{t}{c}\right)(1 + 0.151 \, C_\mu^{1/2} + 0.219 \, C_\mu) \tag{A.8}$$

The solution proceeds by developing, from Equation (A.7), a series of N simultaneous equations where the first N odd terms are applied at N stations along the blown semispan. The coefficients A_n thus acquired provide for:

$$\alpha_{icc} = \frac{w_i \, (\theta_{cc})}{V_\infty} = \sum_{n=1}^{2N} n \, A_n \, \frac{\sin n \, \theta_{cc}}{\sin \theta_{cc}} \tag{A.9}$$

where $A_n = A_1, A_3, A_5 \ldots A_{2N}$.
Equation (A.9), along with (A.5), provides for Equation (A.1)

$$\alpha_{cc} = \alpha'_{cc} - \alpha_{icc}$$

and, hence, for the downwash corrected, circulation induced incidence. It should be noted that Equation (A.9), once obtained, will provide the upwash in the region between the blown portion of the wing and the fuselage.

THREE-DIMENSIONAL SUMMATION

In accordance with the potential flow model, as depicted in Figure 1, the remaining factors of the wing body model are provided for in Equation (5) reduced to:

$$\sum_{n=1}^{\infty} A_n \sin n\theta \, \{n\mu \, [1+f(y)] + \sin \theta\} = \mu (\alpha_g + \alpha_c) \sin \theta \tag{A.10}$$

$$\frac{\delta}{c} = \frac{2\left(\frac{r}{c}\right)}{\pi} \frac{\left[\left(\frac{V_J}{V_\infty} - 1\right)\right]}{\left[1 + \left(\frac{V_J}{V_\infty}\right)\right]}$$

Equation (A.4) becomes:

$$\frac{V_{LE}}{V_\infty} = \frac{\frac{(r_{TE} + \delta)}{c}}{1 + \frac{(r_{TE} + \delta)}{c}} \sqrt{\frac{C_\mu}{\frac{h}{c}}} \tag{A.6}$$

Equations (A.5) and (A.6) then provide the spanwise distribution of the two-dimensional circulation induced incidence.

BLOWING INDUCED DOWNWASH

Considering the blowing segment of the wing as a separate full span wing, a lifting line solution to that segment will provide the downwash correction to the blowing circulation induced incidence of Equation (A.5). The form of the fundamental equation applying to the blown portion of the wing is:

$$\sum_{n=1}^{\infty} A_n \sin n\theta_{cc} (n_\mu + \sin \theta_{cc}) = \mu \, \alpha'_{cc} \sin \theta_{cc} \tag{A.7}$$

where

$$\mu = \frac{a_o}{4} \frac{c}{b_{cc}}$$

and

$$\theta_{cc} = \cos^{-1}\left(\frac{2 \, y_{cc}}{b_{cc}}\right)$$

39

$$r_{TE} \ V_J = (c - r_{TE}) \ V_{LE}$$

or

$$V_{LE} = \frac{\dfrac{r_{TE}}{c}}{1 - \dfrac{r_{TE}}{c}} \ V_J$$

For the usual case of a uniform slot height to chord ratio, the blowing coefficient can be expressed as:

$$C_\mu = 2 \left(\frac{h}{c} \right) \left(\frac{V_J}{V_\infty} \right)^2$$

(For the case of less than full span blowing, the local blowing coefficient is the above multiplied by the ratio of the total wing area to the blown wing area.) Thus we obtain:

$$\frac{V_{LE}}{V_\infty} = \frac{\dfrac{r_{TE}}{c}}{1 - \dfrac{r_{TE}}{c}} \sqrt{\frac{C_\mu}{\dfrac{h}{c}}} \tag{A.4}$$

The circulation induced incidence can then be expressed as:

$$\alpha'_{cc} = \tan^{-1} \left(\frac{V_{LE}}{V_\infty} \right) \tag{A.5}$$

A correction to the trailing edge radius is determined by considering the growth of the trailing edge jet flow with increased blowing. The "discrete vortex" model of the Coanda jet flow proposed by Smith[6] and championed by Wood[7] provides for the jet shear layer growth rate as:

APPENDIX

SPANWISE LIFT DISTRIBUTION FOR BLOWING SEGMENT
OF CIRCULATION CONTROL WING

The configuration being considered here is that of a high aspect ratio wing body with full to partial span trailing edge blowing. It will be assumed that the aspect ratio is sufficiently large that the semispan, or blown portion of the semi-span, can itself be considered as a high aspect ratio wing. The lifting line approach can then be justifiably applied to the isolated blowing segment alone. The vortex pattern for this potential flow model is shown in Figure 1. In this manner the distribution of α_{cc}, as required for Equation (5), will have been modified to account for the downwash effects resulting from the vortex pattern established by the blowing segment alone. This can be expressed as:

$$\alpha_{cc} = \alpha'_{cc} - \alpha_{icc} \qquad (A.1)$$

where α'_{cc} represents the local two-dimensional blowing induced incidence and α_{icc} represents the downwash produced by the blowing segment's trailing vortices.

TWO-DIMENSIONAL CIRCULATION CONTROL INCIDENCE

The reasoning behind the small angle assumption of the lifting line theory will be extended to that of the circulation control airfoil. Based on the known aft loading of a circulation control airfoil, and the geometry of the airfoil itself, Figure 2, the blowing induced incidence, for moderate levels of blowing, will be generated by a point vortex located on the chordline, at a distance of the trailing edge radius, from the trailing edge. The strength of the vortex is provided by the jet velocity and the trailing edge radius.

Hence

$$\Gamma_{vor} = 2\pi \, r_{TE} \, V_j \qquad (A.2)$$

On this basis (and the geometry of Figure 2), it can be expressed as:

37

TABLE 1 - MODEL GEOMETRIC CHARACTERISTICS

Wing

Area	2.2128 ft^2
Span (exluding unblown tips)	75.0 in.
Chord at rotation center;	5.665 in.
at wing tip	2.8325 in.
Mean geometric chord	4.44 in.
Taper ratio	0.50
Aspect ratio	17.65
Blowing slot height	0.002c
Slot location	0.968c
Root section	CC20/05/053/97-E
Tip section	CC15/00/022/97-E
Left wing slot exit area	0.00206 ft^2
Right wing slot exit area	0.00198 ft^2
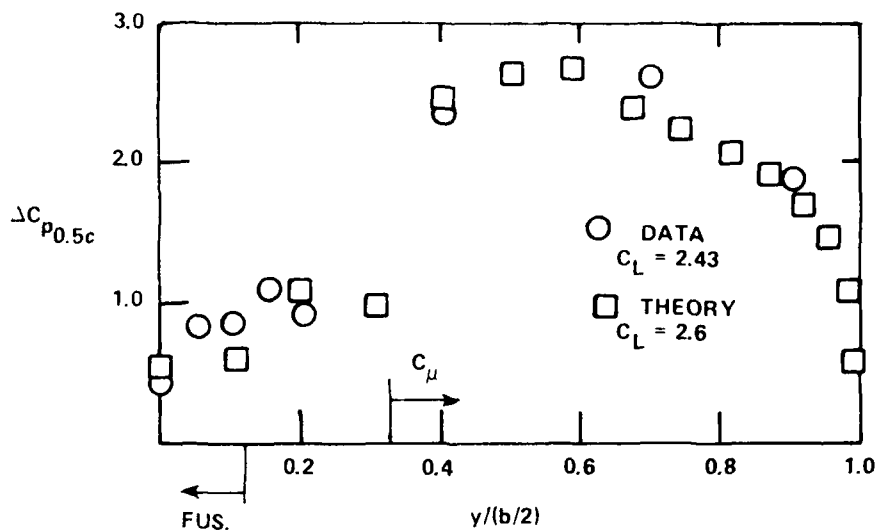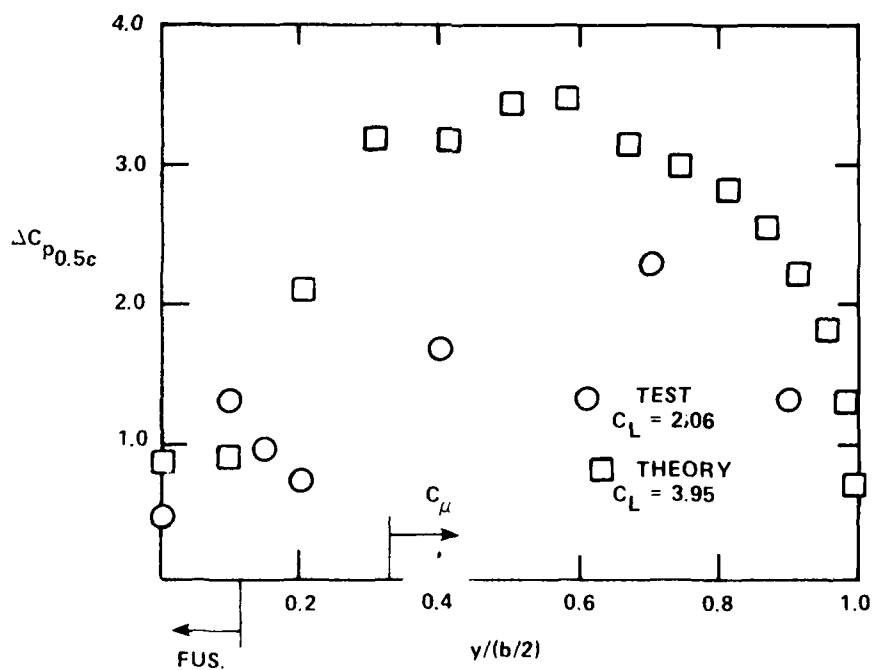
Figure 29 – Span Lift Distribution, Configuration 4,
C_μ = 0.105 and 0.268

34
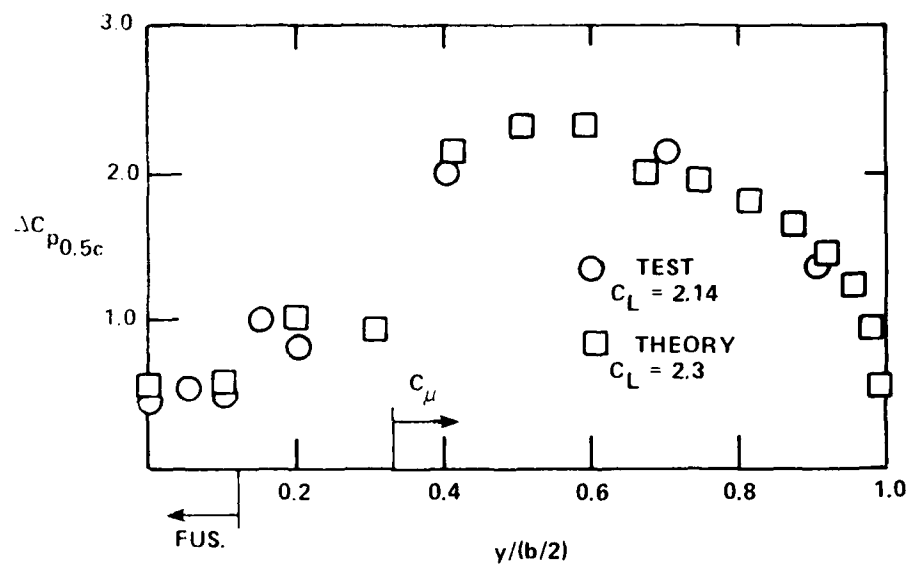
$C_\mu = 0.08$, $\alpha = 3.35$ deg $= 0.0585$ rad
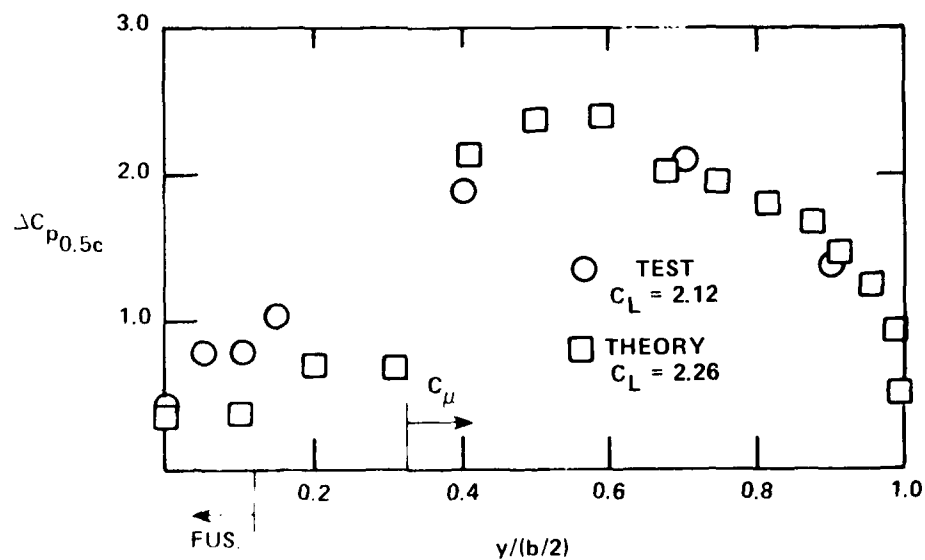
$C_\mu = 0.104$, $\alpha = 0.33$ deg $= 0.0057$ rad

Figure 28 – Span Lift Distribution, Configuration 4,
$C_\mu = 0.08$ and 0.104
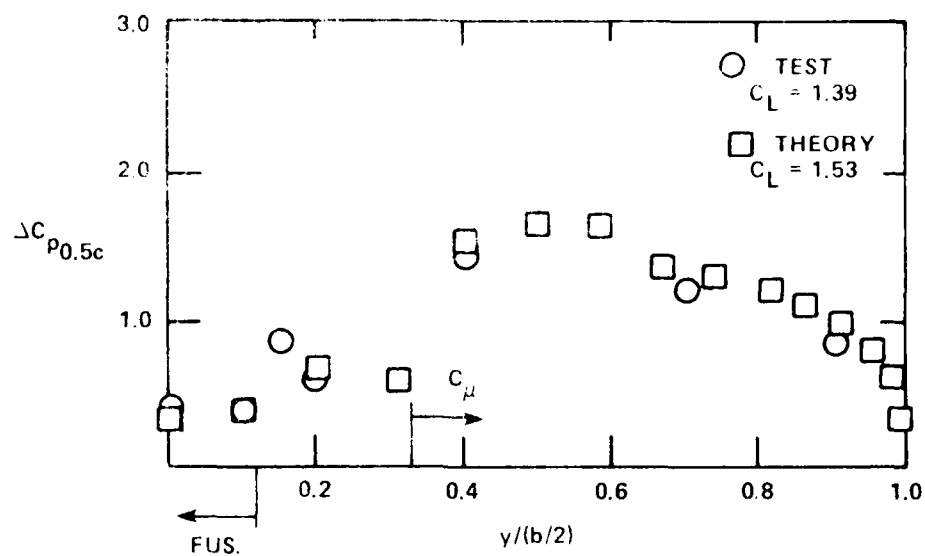
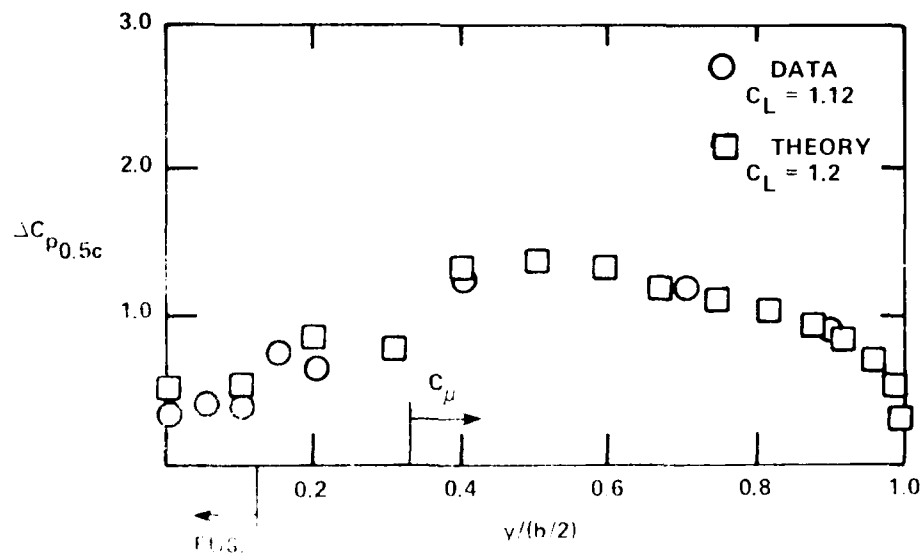Figure 27 - Span Lift Distribution, Configuration 4,
$C_\mu = 0.024$ and 0.051

END

FILMED

8-85

DTIC